J|A|C|S
ARTICLES
Published on Web 03/09/2007

Structural and Photophysical Properties of Adducts of $[Ru(bipy)(CN)_4]^{2-}$ with Different Metal Cations: Metallochromism and Its Use in Switching Photoinduced Energy Transfer

Theodore Lazarides,[†] Timothy L. Easun,[†] Claire Veyne-Marti,[†] Wassim Z. Alsindi,[‡] Michael W. George,[‡] Nina Deppermann,[†] Christopher A. Hunter,[†] Harry Adams,[†] and Michael D. Ward*,[†]

Contribution from the Department of Chemistry, University of Sheffield, Sheffield S3 7HF, United Kingdom, and School of Chemistry, University of Nottingham, University Park, Nottingham NG7 2RD, United Kingdom

Received November 30, 2006; E-mail: m.d.ward@sheffield.ac.uk

Abstract: We show in this paper how the ^{3}MLCT luminescence of $[Ru(bipy)(CN)_4]^{2-}$, which is known to be highly solvent-dependent, may be varied over a much wider range than can be achieved by solvent effects, by interaction of the externally directed cyanide ligands with additional metal cations both in the solid state and in solution. A series of crystallographic studies of $[Ru(bipy)(CN)_4]^{2-}$ salts with different metal cations M^{n+} (Li^+, Na^+, K^+, mixed Li^+/K^+, Cs^+, and Ba^{2+}) shows how the cyanide/M^{n+} interaction varies from the conventional "end-on" with the more Lewis-acidic cations (Li^+, Ba^{2+}) to the more unusual "side-on" interaction with the softer metal cations (K^+, Cs^+). The solid-state luminescence intensity and lifetime of these salts is highly dependent on the nature of the cation, with Cs^+ affording the weakest luminescence and Ba^{2+} the strongest. A series of titrations of the more soluble derivative $[Ru(^tBu_2bipy)(CN)_4]^{2-}$ in MeCN with a range of metal salts showed how the cyanide/M^{n+} association results in a substantial blue-shift of the ^{1}MLCT absorptions, and ^{3}MLCT energies, intensities, and lifetimes, with the complex varying from essentially non-luminescent in the absence of metal cation to showing strong ($\phi = 0.07$), long-lived (1.4 μs), and high-energy (583 nm) luminescence in the presence of Ba^{2+}. This modulation of the ^{3}MLCT energy, over a range of about 6000 cm^{-1} depending on the added cation, could be used to reverse the direction of photoinduced energy transfer in a dyad containing covalently linked $[Ru(bipy)_3]^{2+}$ and $[Ru(bipy)(CN)_4]^{2-}$ termini. In the absence of a metal cation, the $[Ru(bipy)(CN)_4]^{2-}$ terminus has the lower ^{3}MLCT energy and thereby quenches the $[Ru(bipy)_3]^{2+}$-based luminescence; in the presence of Ba^{2+} ions, the ^{3}MLCT energy of the $[Ru(bipy)(CN)_4]^{2-}$ terminus is raised above that of the $[Ru(bipy)_3]^{2+}$ terminus, resulting in energy transfer to and sensitized emission from the latter.

Introduction

The luminescent complex $[Ru(bipy)(CN)_4]^{2-}$ [1,2] has been known for some time to be strongly solvatochromic,[3] with both its ^{1}MLCT absorption and its ^{3}MLCT emission spectra being tunable over a wide range in different solvents. This phenomenon arises from hydrogen-bonding interactions of the externally directed cyanide lone pairs with solvents that are good hydrogen-bond donors. Thus, in non-hydrogen-bonding solvents such as acetone or DMSO, $[Ru(bipy)(CN)_4]^{2-}$ is purple with the ^{1}MLCT absorption maximum at ca. 550 nm, and the associated ^{3}MLCT luminescence at ca. 800 nm is very weak and short-lived. In water, however, the MLCT states are much higher in energy, with the ^{1}MLCT absorption maximum shifted to 400 nm and the associated ^{3}MLCT luminescence being much stronger ($\lambda_{em} = 620$ nm, $\tau = 100$ ns).[1-3] A similar effect can be obtained in non-hydrogen-bonding solvents by addition of protonated poly amine macrocycles; the array of cationic N−H groups interacts with the cyanide ligands and provides a hydrogen-bonding environment comparable to that which occurs in water.[4]

The effect has been exploited as the basis of a switching effect in dyads that combine a $[Ru(bipy)(CN)_4]^{2-}$ unit with some other energy-donor or -acceptor component whose energy levels are essentially solvent independent,[5,6] because changing the solvent can make the ^{3}MLCT energy of the $[Ru(bipy)(CN)_4]^{2-}$ unit be higher or lower than that of an adjacent chromophore such as

[†] University of Sheffield.
[‡] University of Nottingham.

(1) (a) Bignozzi, C. A.; Chiorboli, C.; Indelli, M. T.; Scandola, M. A. R.; Varani, G.; Scandola, F. *J. Am. Chem. Soc.* **1986**, *108*, 7872. (b) Habib Jiwan, J. L.; Wegewijs, B.; Indelli, M. T.; Scandola, F.; Braslavsky, S. E. *Recl. Trav. Chim. Pays-Bas* **1995**, *114*, 542.
(2) Ward, M. D. *Coord. Chem. Rev.* **2006**, *250*, 3128.
(3) Timpson, C. J.; Bignozzi, C. A.; Sullivan, B. P.; Kober, E. M.; Meyer, T. J. *J. Phys. Chem.* **1996**, *100*, 2915.
(4) Pina, F.; Parola, A. J. *Coord. Chem. Rev.* **1999**, *185−186*, 149.
(5) Simpson, N. R. M.; Ward, M. D.; Morales, A. F.; Barigelletti, F. *J. Chem. Soc., Dalton Trans.* **2002**, 2449.
(6) Indelli, M. T.; Ghirotti, M.; Prodi, A.; Chiorboli, C.; Scandola, F.; McClenaghan, N. D.; Puntoriero, F.; Campagna, S. *Inorg. Chem.* **2003**, *42*, 5489.

 10.1021/ja068436n CCC: $37.00

$[Ru(bipy)_3]^{2+}$ (ref 5) or pyrene.[6] In water, therefore, the $[Ru(bipy)(CN)_4]^{2-}$ unit acts as the energy-donor and will sensitize chromophores with lower-lying emissive states; but in, for example, MeCN it acts as the energy-acceptor and quenches luminescence from the same chromophores. Photoinduced energy transfer is an essential feature of light-harvesting antenna systems for solar energy conversion[7] and may also be an essential step in molecular electronic devices, whereby information (in the form of excitation energy) is transferred from one point to another.[8] Thus, long-range energy transfer may fulfill, in light-based systems where input and output consist of photons, a function analogous to that of the transfer of electrons through wires in conventional electronic circuits. In this context, the ability to change the direction of PEnT back and forth constitutes an important switching function, allowing preparation of devices that are one step more sophisticated than simple "wires".[9]

Given that a protic solvent has such a substantial effect on the ^{3}MLCT energy of $[Ru(bipy)(CN)_4]^{2-}$, arising from coordination of the cyanide lone pairs to the $\delta+$ H atoms of the solvent, we reasoned that coordination of the cyanide lone pairs to a metal cation should have a similar, or greater, effect. This could provide an alternative means of controlling the energy of the ^{3}MLCT state of the $[Ru(bipy)(CN)_4]^{2-}$ unit: in non-hydrogen-bonding solvents, addition of soluble metal salts could result in Ru−CN−M^{n+} interactions, raising the ^{3}MLCT energy of the of $[Ru(bipy)(CN)_4]^{2-}$ chromophore and increasing its luminescence intensity and lifetime. The effect by which the optical properties of dye molecules are perturbed in interaction with metal cations has been termed "metallochromism",[10] a term which is applied in this work to changes in luminescence as well as absorption properties.

Our recent crystallographic investigations have showed that $[Ru(bipy)(CN)_4]^{2-}$ and its relatives crystallize as coordination networks with a range of metal ions, with two distinct types of interaction between the cyanide ligand and the metal cation.[11] With "hard" metal ions such as lanthanide(III) ions (Ln^{3+}), the cyanides of $[Ru(bipy)(CN)_4]^{2-}$ coordinate in an end-on manner to give near-linear Ru−CN−Ln bridges.[11] With the softer cation K^+, side-on interactions can also form in which the electron density in the triple bond interacts with the K^+ center to give an η^2-type coordination mode, similar to that of an alkyne coordinating to a low oxidation state transition metal center (although the interaction is primarily electrostatic in origin).[11a,b] It is obvious from these studies that $[Ru(bipy)(CN)_4]^{2-}$ provides extensive possibilities for novel structural chemistry by interacting in different ways with metal cations of different size and charge; and, as we show, these interactions have a significant effect on the photophysical properties of the $[Ru(bipy)(CN)_4]^{2-}$ chromophore.

Accordingly, we describe in this paper the interaction of $[Ru(bipy)(CN)_4]^{2-}$ and a substituted derivative with a range of metal cations both in the solid state and in solution, and we show how the resultant modulation of the photophysical properties of the $[Ru(bipy)(CN)_4]^{2-}$ unit can be used as the basis of switching inter-component photoinduced energy transfer in a dyad system. This paper is divided into four parts. First, we describe X-ray crystallographic investigations of a range of $[Ru(bipy)(CN)_4]^{2-}/M^{n+}$ salts, which show the effect of the size and charge of M^{n+} on the nature of the CN^-/M^{n+} interaction and hence the structures of the compounds. Second, we describe photophysical studies on $[Ru(bipy)(CN)_4]^{2-}/M^{n+}$ salts in the solid state, which show how metal ions affect the properties of $[Ru(bipy)(CN)_4]^{2-}$ to different extents depending on their size and charge. Third, solution spectroscopic titrations of the soluble derivative $[Ru(^tBu_2bipy)(CN)_4]^{2-}$ with a range of different metal cations were performed to see the extent to which interaction of its cyanide ligands with additional metal ions affected its photophysical properties in solution. Fourth, we describe the synthesis and photophysical properties of a $[Ru(bipy)(CN)_4]^{2-}/[Ru(bipy)_3]^{2+}$ dyad in which modulation of the ^{3}MLCT energy of the $[Ru(bipy)(CN)_4]^{2-}$ center by interaction with Ba^{2+} ions, following the principles explained in the first three sections, allows the direction of photoinduced energy transfer between the components to be reversed.

Results and Discussion

(i) Structures of Salts of $[Ru(bipy)(CN)_4]^{2-}$ with Different Cations. We crystallized $[Ru(bipy)(CN)_4]^{2-}$ from aqueous solutions in the presence of a large excess of a range of different metal salts (Li^+, Na^+, K^+, Cs^+, Ba^{2+}). The resulting series of structures show very clearly how the nature of the interaction between the cyanide ligand and the metal cation M^{n+} depends on the charge:radius ratio of M^{n+}. The crystallographic, data collection, and refinement parameters, and lists of bond lengths and angles, are in the Supporting Information.

The structure of $Li_2[Ru(bipy)(CN)_4]\cdot(H_2O)_6$ is in Figure 1; the complex anion and both Li cations lie on two-fold symmetry axes such that the asymmetric unit contains one-half of the molecular formula unit. Each $[Ru(bipy)(CN)_4]^{2-}$ anion interacts with two Li^+ cations [Li(1) and its symmetry equivalent Li(1A)], via end-on Ru−CN−Li bridges using the two cyanide ligands that are in the same plane as the bipy ligand (Figure 2). The C(12)−N(4)−Li(1) angle (139°) is considerably distorted from linearity. Each Li(1) center in turn is coordinated by two cyanide ligands [via atom N(4)] from adjacent $[Ru(bipy)(CN)_4]^{2-}$ anions, forming a one-dimensional chain of alternating $[Ru(bipy)(CN)_4]^{2-}$ anions and Li^+ cations; each of these Li^+

(7) (a) Bignozzi, C. A.; Argazzi, R.; Kleverlaan, C. J. *Chem. Soc. Rev.* **2000**, *29*, 87. (b) Roger, C.; Muller, M. G.; Lysetska, M.; Miloslavina, Y.; Holzwarth, A. R.; Wurthner, F. *J. Am. Chem. Soc.* **2006**, *128*, 6542. (c) Burrell, A. K.; Officer, D. L.; Plieger, P. G.; Reid, D. C. W. *Chem. Rev.* **2001**, *101*, 2751. (d) Balzani, V.; Ceroni, P.; Juris, A.; Venturi, M.; Campagna, S.; Puntoriero, F.; Serroni, S. *Coord. Chem. Rev.* **2001**, *219*, 545. (e) Campagna, S.; Di Pietro, C.; Loiseau, F.; Maubert, B.; McClenaghan, N.; Passalacqua, R.; Puntoriero, F.; Ricevuto, V.; Serroni, S. *Coord. Chem. Rev.* **2001**, *229*, 67. (f) Guldi, D. M. *Chem. Soc. Rev.* **2002**, *31*, 22.
(8) (a) Jukes, R. T. F.; Adamo, V.; Hartl, F.; Belser, P.; De Cola, L. *Coord. Chem. Rev.* **2005**, *249*, 1327. (b) Welter, S.; Lafolet, F.; Cecchetto, E.; Vergeer, F.; De Cola, L. *ChemPhysChem* **2005**, *6*, 2417. (c) Low, P. J. *Dalton Trans.* **2005**, 2821. (d) Coe, B. J.; Curati, N. R. M. *Comments Inorg. Chem.* **2004**, *25*, 147. (e) Venturi, M.; Balzani, V.; Ballardini, R.; Credi, A.; Gandolfi, M. T. *Int. J. Photoenergy* **2004**, *6*, 1. (f) Burrell, A. K.; Wasielewski, M. R. *J. Porphyrins Phthalocyanines* **2000**, *4*, 401.
(9) (a) Gust, D.; Moore, T. A.; Moore, A. L. *Chem. Commun.* **2006**, 1169. (b) Kuhni, J.; Adamo, V.; Belser, P. *Chimia* **2006**, *60*, 207. (c) Raymo, F. M.; Tomasulo, M. *Chem. Soc. Rev.* **2005**, *34*, 327. (d) Sans, M. Q.; Belser, P. *Coord. Chem. Rev.* **2002**, *229*, 59. (e) Ward, M. D. *J. Chem. Educ.* **2001**, *78*, 321.
(10) (a) Kovtun, Y. P.; Prostota, Y. O.; Tolmachev, A. I. *Dyes Pigm.* **2003**, *58*, 83. (b) Kubo, Y. *J. Chem. Soc., Perkin Trans. 1* **1994**, 1787.
(11) (a) Davies, G. M.; Pope, S. J. A.; Adams, H.; Faulkner, S.; Ward, M. D. *Inorg. Chem.* **2005**, *44*, 4656. (b) Adams, H.; Alsindi, W. Z.; Davies, G. M.; Duriska, M. B.; Easun, T. L.; Fenton, H. E.; Herrera, J.-M.; George, M. W.; Ronayne, K. L.; Sun, X.-Z.; Towrie, M.; Ward, M. D. *Dalton Trans.* **2006**, 39. (c) Herrera, J.-M.; Baca, S.; Adams, H.; Ward, M. D. *Polyhedron* **2006**, *25*, 869. (d) Herrera, J.-M.; Pope, S. J. A.; Adams, H.; Faulkner, S.; Ward, M. D. *Inorg. Chem.* **2006**, *45*, 3895. (e) Herrera, J.-M.; Ward, M. D.; Adams, H.; Pope, S. J. A.; Faulkner, S. *Chem. Commun.* **2006**, 1851. (f) Baca, S. G.; Adams, H.; Ward, M. D. *Cryst. Eng. Commun.* **2006**, *8*, 635.

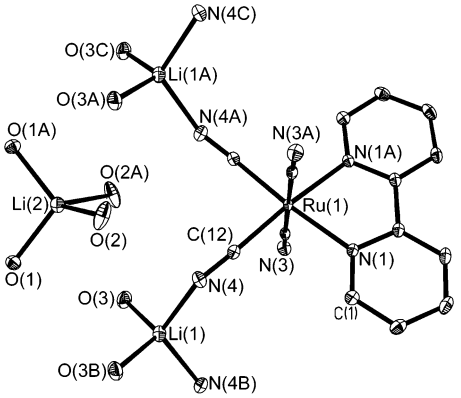

Figure 1. Crystal structure of the repeat unit of $Li_2[Ru(bipy)(CN)_4]\cdot(H_2O)_6$; the atoms Ru(1), Li(1), and Li(2) all lie on C_2 axes. Thermal ellipsoids are at the 40% probability level.

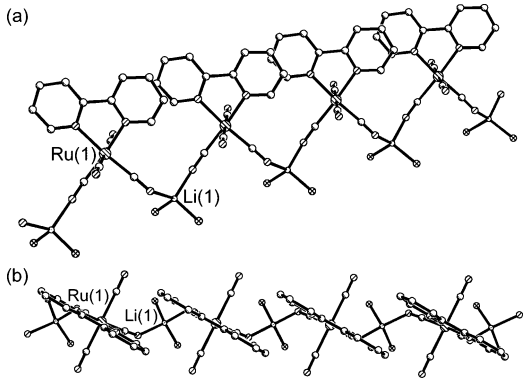

Figure 2. Two views of the alternating cyanide-bridged Ru/Li chain in $Li_2[Ru(bipy)(CN)_4]\cdot(H_2O)_6$.

cations [Li(1)] is also coordinated by two water molecules, giving an approximately tetrahedral N_2O_2 coordination environment. The bipy ligands of adjacent $[Ru(bipy)(CN)_4]^{2-}$ anions in the chain partially overlap such that each bipy ligand is π-stacked with its neighbors with a separation of 3.37 Å between the parallel, overlapping ring segments. Charge balance is provided by a separate tetrahedral $[Li(H_2O)_4]^+$ complex cation in the lattice, which interacts with the main chain via hydrogen-bonding interactions (e.g., O(2)···O(3A) 2.94 Å, OH···O angle 167°). In addition, the axial cyanide N atom [N(3)] forms hydrogen bonds with three water molecules that are coordinated to other Li^+ centers [N(3)···O(1B) 2.84 Å, OH−N angle 174°; N(3)···O(1C) 3.01 Å, OH−N angle 174°; and N(3)···O(3B) 2.99 Å, OH−N angle 166°].

The structure of $K_2[Ru(bipy)(CN)_4]\cdot(H_2O)_3$ is shown in Figures 3 and 4. It is clear in this structure how the "softer" K^+ ions, with their larger ionic radius, prefer to interact with the cyanide donors in a side-on rather than an end-on coordination mode. All four cyanide ligands are involved in side-on binding to varying numbers of K^+ ions: for the cyanide ligands containing N atoms N(3), N(4), N(5), and N(6), the number of such side-on interactions to different K^+ ions is two, two, three, and one, respectively [Figure 3a]. The cyanide group containing N(5) is also involved in an end-on Ru−CN−K cyanide bridge. The side-on cyanide/K^+ interactions involve rather long K−C and K−N contacts, averaging 3.20 and 3.01 Å, respectively, with acute C−K−N angles associated with each cyanide group (19−22°); it is noticeable that the cyanides are in general not exactly "edge-on" (with equal K−C and K−N distances) but

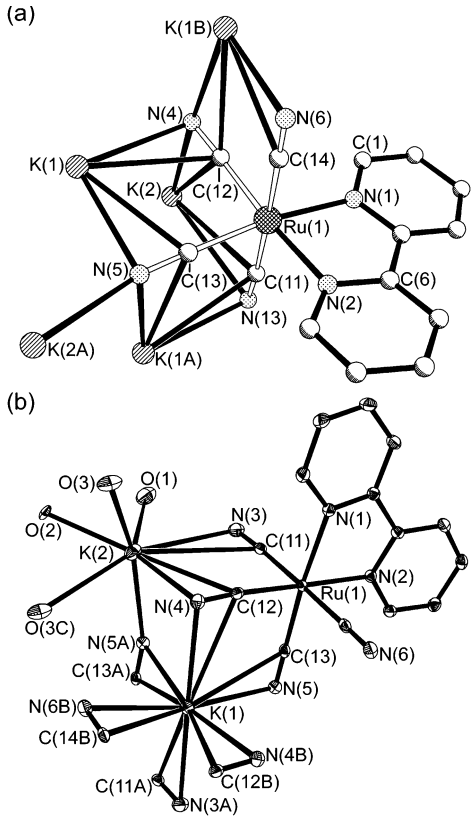

Figure 3. Two views of part of the coordination network structure in $K_2[Ru(bipy)(CN)_4]\cdot(H_2O)_3$: part (a) emphasizes the coordination environment around each $[Ru(bipy)(CN)_4]^{2-}$ anion, with all interacting K^+ ions shown (the cyanide ligands are shown with hollow bonds for clarity); part (b) shows the complete coordination environment around each K^+ center. Thermal ellipsoids are at the 40% probability level.

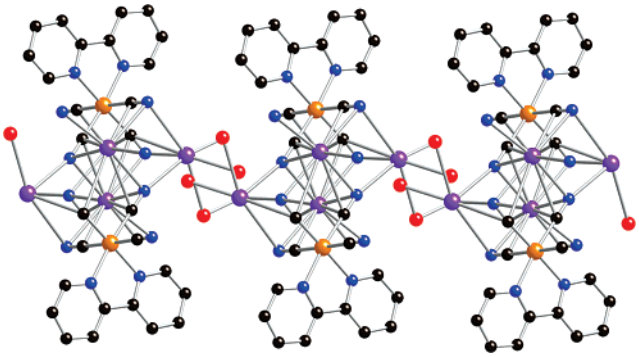

Figure 4. View of the structure of $K_2[Ru(bipy)(CN)_4]\cdot(H_2O)_3$ looking edge-on at a two-dimensional sheet down the crystallographic *a*-axis (K, purple; O, red; N, blue; Ru, orange; C, black).

are slightly slanted so that the more electronegative N atoms of the cyanides are closer to the K^+ ions than are the associated C atoms. The coordination environments around K(1) and K(2) are shown in Figure 3b. K(1) is side-on bound by six cyanide ligands whose centers define a roughly octahedral array; K(2) in contrast has only two such side-on cyanide ligands, one conventional terminal cyanide ligand [N(5A)], and four water ligands. The result is a complicated two-dimensional coordination network structure (Figure 4) in which chains of $[Ru(bipy)(CN)_4]^{2-}$ anions and K(1) cations, aligned along the crystallographic *a*-axis (and receding into the page in the view in Figure 4), are cross-linked via bridging water ligands that connect K(2) cations located at the edge of each chain.

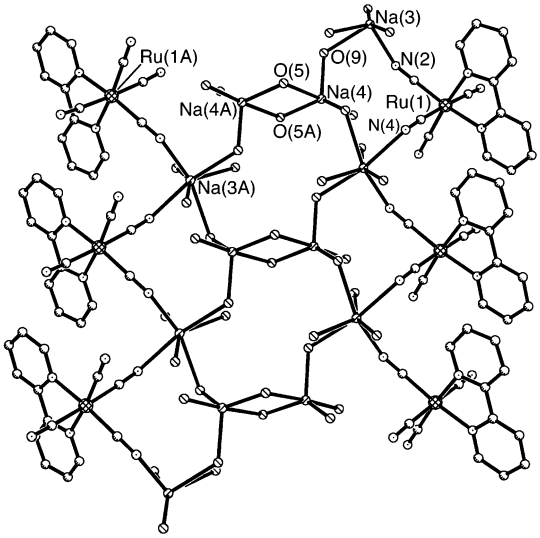

Figure 5. Crystal structure of $Na_2[Ru(bipy)(CN)_4]\cdot(H_2O)_9$, showing one of the two disorder components involving the Na^+ ions and their associated water ligands. Na(3) and Na(4) have only 50% site occupancy.

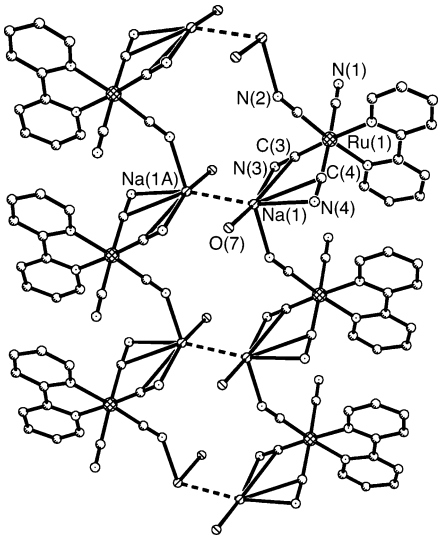

Figure 6. Crystal structure of $Na_2[Ru(bipy)(CN)_4]\cdot(H_2O)_9$, showing the alternate disorder component involving the Na^+ ions and their associated water ligands. Na(1) has only 50% site occupancy; Na(2) is coordinated only by water ligands and lies between adjacent chains (not shown for clarity). The Na···Na contacts indicated by dotted lines in this figure are an artifact of the disorder; because only 50% of the Na(1) sites are occupied, these apparently short Na···Na interactions will not actually occur.

Crystals of $Na_2[Ru(bipy)(CN)_4]\cdot(H_2O)_9$ (Figures 5 and 6) proved to have substantial disorder of the two Na^+ ions and most of their associated water ligands; accordingly, the structure is more difficult to describe, which is why it is presented out of sequence, that is, after the Li^+ and K^+ structures. The general structure is that of ladder-like one-dimensional chains, with two columns of $[Ru(bipy)(CN)_4]^{2-}$ anions separated by a network of water-bridged Na^+ ions. There are four sites for Na^+ ions, each of which has a site occupancy of 50%. The interaction of the $[Ru(bipy)(CN)_4]^{2-}$ units involves either end-on cyanide ligation to Na(3), as in Figure 5, or a combination of side-on and end-on ligation to Na(1), as in Figure 6. The side-on cyanide interactions (Figure 6) involve Na−N separations of 2.85 and 2.88 Å to N(4) and N(3), respectively, and slightly longer bonds to the associated carbon atoms [3.05 and 3.03 Å to C(4) and C(3), respectively], as we saw above in the K^+ structure. In

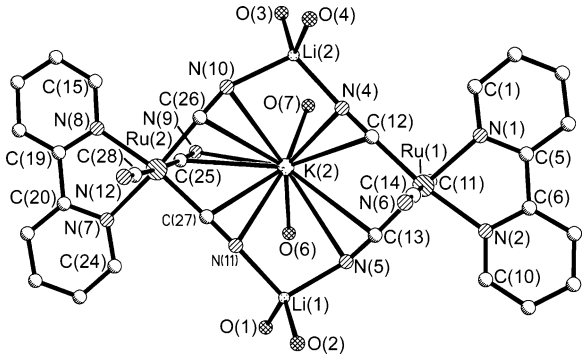

Figure 7. Part of the asymmetric unit of $KLi[Ru(bipy)(CN)_4]\cdot(H_2O)_4$ [atom K(1) and its associated water ligands are not shown for clarity].

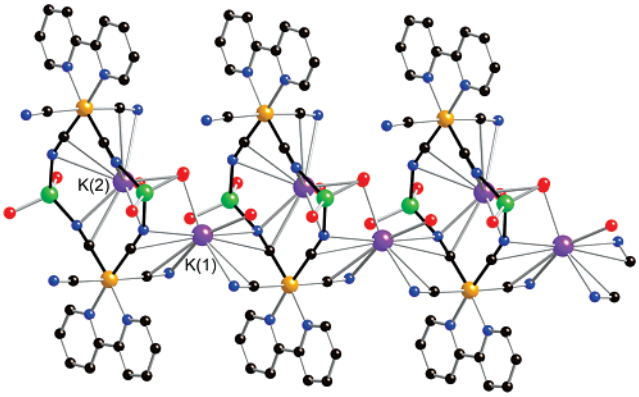

Figure 8. View of the chain structure of $KLi[Ru(bipy)(CN)_4]\cdot(H_2O)_4$, showing how the $Ru_2Li_2(\mu\text{-}CN)_4$ squares (which are highlighted with black bonds), each with a "capping" K(2) ion, are cross-linked by K(1) ions via edge-on cyanide interactions (K, purple; Li, green; O, red; N, blue; Ru, orange; C, black).

contrast, the "end-on" interactions involve shorter Na−N distances, for example, 2.56 Å for Na(1)−N(2) [shown in Figure 6] and 2.45 and 2.61 Å from Na(3) to N(2) and N(4) [shown in Figure 5]. It is only Na(1) and Na(3) that interact directly with the $[Ru(bipy)(CN)_4]^{2-}$ anion, in either an end-on or a side-on manner; Na(2) and Na(4) are coordinated solely by water molecules. Given the difficulty in assigning fractional occupancy water molecules to specific fractional Na^+ cations, a more detailed discussion of the coordination geometries and bond lengths about the Na^+ ions is inappropriate. The main point to note for this structure is that in contrast to the Li^+ structure it contains examples of side-on cyanide bridging, but side-on coordination is not as prevalent as it is in the K^+ structure. Accordingly, the Na^+ cations are displaying behavior intermediate between Li^+ and K^+ in their interactions with cyanide ligands.

The difference in the mode of interaction of "hard" and "soft" metal cations with $[Ru(bipy)(CN)_4]^{2-}$ is nicely demonstrated in the structure of the mixed salt $KLi[Ru(bipy)(CN)_4]\cdot(H_2O)_4$ (Figures 7 and 8), which was isolated in small amounts during attempts to prepare the Li^+ salt $Li_2[Ru(bipy)(CN)_4]\cdot(H_2O)_6$ by crystallization of the potassium salt $K_2[Ru(bipy)(CN)_4]\cdot(H_2O)_3$ from an aqueous solution containing excess LiCl. Figure 7 shows part of the asymmetric unit, consisting of two independent $[Ru(bipy)(CN)_4]^{2-}$ anions, two independent Li^+ cations, and one of the two K^+ cations. The two $[Ru(bipy)(CN)_4]^{2-}$ anions each coordinate their two cyanides which are in the same plane as the bipyridine ligand to a separate Li^+ ion each, in an end-on manner, generating an approximate Ru_2Li_2 square based on Ru−

CN−Li edges. Each Li^+ ion is approximately tetrahedrally coordinated, by two cyanide N atoms (one from each $[Ru(bipy)(CN)_4]^{2-}$ unit, average Li−N separation 2.04 Å) and two water ligands (average Li−O separation, 1.92 Å). A K^+ ion [K(2)] lies above this square, coordinated "side-on" by the four cyanide ligands around the edges of the square and also by a fifth cyanide ligand [one of the axial ligands on the Ru(II) centers, which is not involved in the $Ru_2Li_2(\mu\text{-}CN)_4$ square structure]; K(2) also has two water ligands. Similarly, K(1) is bound side-on by four cyanide ligands from two different (but symmetry equivalent) $[Ru(bipy)(CN)_4]^{2-}$ anions, and therefore links two adjacent $Ru_2Li_2(\mu\text{-}CN)_4$ squares; K(1) also carries three water ligands. The average K−C and K−N separations in these side-on interactions with cyanide ligands are 3.28 and 3.14 Å, respectively, with the same pattern we observed earlier that the K−N interactions are slightly shorter than the K−C interactions. In short, all of the cyanide/Li^+ interactions are end-on, and all of the cyanide/K^+ interactions are side-on, in keeping with what was observed in the crystals of the pure Li^+ and K^+ salts described above. Figure 8 shows how the structure propagates into a one-dimensional coordination network along the crystallographic *a*-axis, with each $Ru_2Li_2(\mu\text{-}CN)_4$ square and its associated "capping" K(2) ion connected by the K(1) ions that link adjacent $Ru_2Li_2(\mu\text{-}CN)_4$ squares.

$Cs_2[Ru(bipy)(CN)_4]\cdot(H_2O)_2$ has a structure that is generally similar to that of $K_2[Ru(bipy)(CN)_4]\cdot(H_2O)_3$ in that the interactions of cyanide ligands with the Cs^+ cations are principally "side-on". The cyanide ligands containing atoms N(3), N(4), N(5), and N(6) interact in this manner with one, two, three, and two Cs^+ cations, respectively; in addition, both N(4) and N(5) each have an additional end-on interaction with another Cs^+ cation (although these C−N−Cs interactions are far from linear). These interactions are illustrated in Figure 9a. Figure 9b shows only the two Cs^+ cations in the asymmetric unit, but with their full coordination spheres. Thus, Cs(2) is in an environment similar to that of K(1) in the structure of $K_2[Ru(bipy)(CN)_4]\cdot(H_2O)_3$ (above), with six side-on cyanide ligands disposed in an approximately octahedral array, but (unlike the K^+ analogue) there is also a water ligand bridging to Cs(1). Cs(1) in contrast has only two side-on cyanide ligands, with two additional water ligands and two N atom donors from end-on bridging cyanides. The average Cs−C and Cs−N distances for the side-on cyanide ligands are 3.60 and 3.37 Å, repeating the pattern we saw earlier that the cyanide ligands are not perfectly "side-on" to the Cs^+ ions but have shorter Cs−N than Cs−C distances. The result of all this cross-linking via bridging cyanide groups is a two-dimensional sheet-like coordination network, consisting of chains of $[Ru(bipy)(CN)_4]^{2-}$ anions and Cs(2) cations oriented along the crystallographic *a*-axis (receding into the page in the view in Figure 10), which are cross-linked by the Cs(1) cations that lie between these chains.

In $Ba[Ru(bipy)(CN)_4]\cdot(H_2O)_6$, the metal cation has a radius similar to that of K^+ but, of course, twice the charge; this results in coordination of the cyanide ligands to Ba^{2+} occurring in an "end-on" mode like that observed for the Li^+ salt (Figure 11). Each $[Ru(bipy)(CN)_4]^{2-}$ units uses the two cyanide ligands that are in the plane of the bipy ligand [containing N(4) and N(5)] to bind to a separate Ba^{2+} center each. Each Ba^{2+} is accordingly coordinated by two end-on cyanide (average Ba−N separation, 2.83 Å) and seven water ligands (average Ba−O separation,

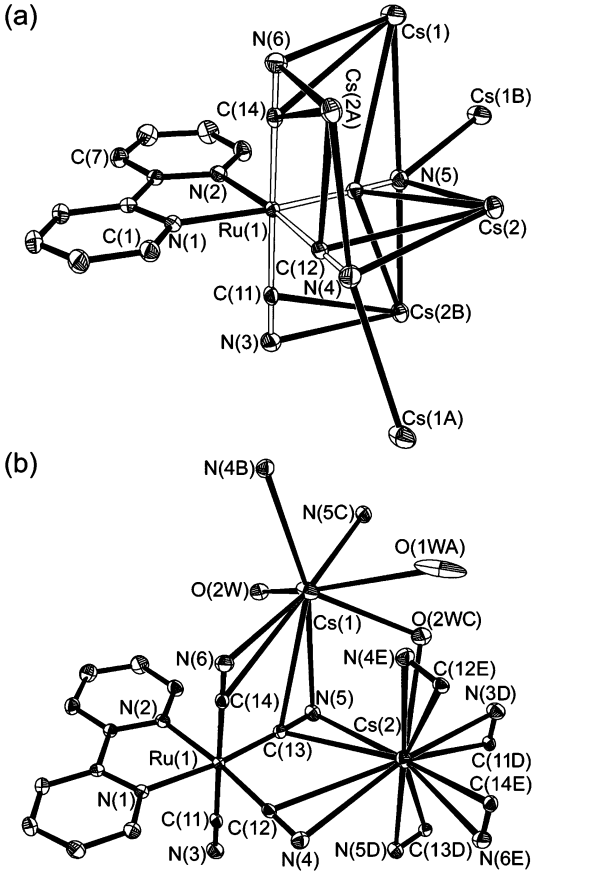

Figure 9. Two views of part of the coordination network structure in $Cs_2[Ru(bipy)(CN)_4]\cdot(H_2O)_2$: part (a) emphasizes the coordination environment around each $[Ru(bipy)(CN)_4]^{2-}$ anion, with all interacting Cs^+ ions shown (the cyanide ligands are shown with hollow bonds for clarity); part (b) shows the complete coordination environment around each Cs^+ center. Thermal ellipsoids are at the 40% probability level.

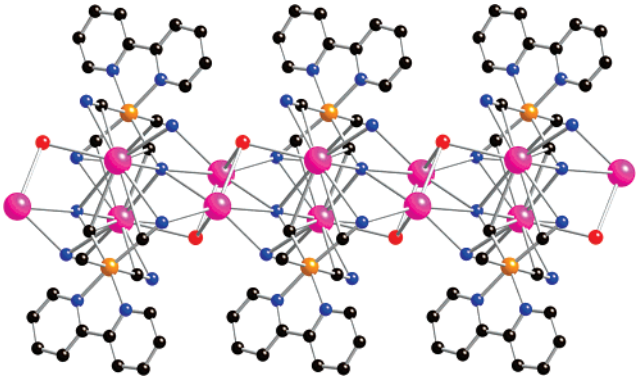

Figure 10. View of the structure of $Cs_2[Ru(bipy)(CN)_4]\cdot(H_2O)_2$ looking edge-on at a two-dimensional sheet down the crystallographic *a*-axis (Cs, pink; O, red; N, blue; Ru, orange; C, black).

2.81 Å). Two of the water ligands [O(3) and its symmetry equivalent] act as bridges between adjacent Ba^{2+} centers, forming a $\{Ba(H_2O)_5\}_2(\mu\text{-}H_2O)_2$ unit. The result is a one-dimensional chain structure in which a sequence of discrete water-bridged Ba^{2+} dimers, running along the center of the chain, is connected by two sequences of $[Ru(bipy)(CN)_4]^{2-}$ units, which lie at the outside edges of the chain (Figure 12); there are clear similarities with the one-dimensional ladder-like structure of $Na_2[Ru(bipy)(CN)_4]\cdot(H_2O)_9$ (Figure 5). The "axial" cyanide ligands [containing N(3) and N(6)] of each $[Ru(bipy)(CN)_4]^{2-}$ unit that are not involved in coordination to Ba^{2+} ions are acting

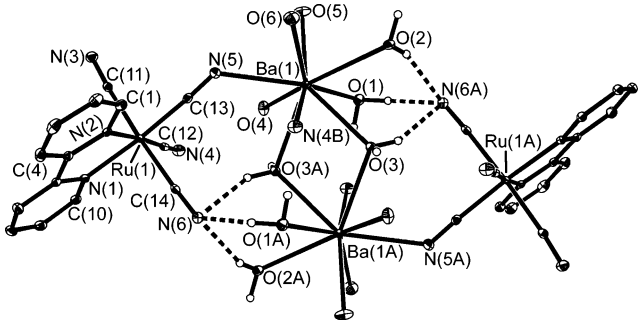

Figure 11. Part of the chain structure of $Ba[Ru(bipy)(CN)_4]\cdot(H_2O)_6$ (the two halves are related by an inversion center). The dotted lines indicate short O···N contacts between water molecules and a cyanide group, indicative of OH−N hydrogen-bonding interactions. Thermal ellipsoids are at the 40% probability level.

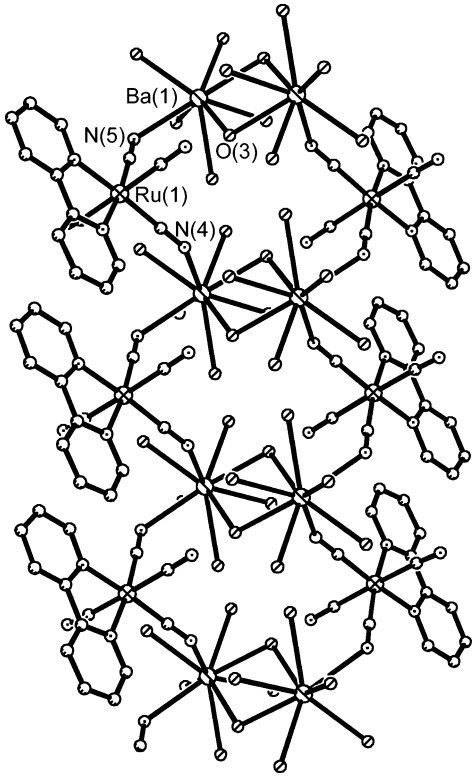

Figure 12. The chain structure of $Ba[Ru(bipy)(CN)_4]\cdot(H_2O)_6$.

as hydrogen-bond acceptors from water molecules, which are themselves coordinated to the $\{Ba(H_2O)_5\}_2(\mu\text{-}H_2O)_2$ units. Thus, N(3) interacts with both O(2) and O(5) from an adjacent asymmetric unit, with nonbonded N···O separations of 2.89 and 2.84 Å, respectively; N(6) interacts with O(1), O(2), and O(3) from the same asymmetric unit, with nonbonded N···O separations of 2.90, 2.92, and 3.04 Å, respectively (these are marked on Figure 11 as dotted lines).

To conclude this section, this set of structures shows a very clear relationship between the coordination mode of the metal cation with the cyanide ligands of $[Ru(bipy)(CN)_4]^{2-}$, and the charge:radius ratio of the cation, with small/"hard" cations giving end-on binding and large/"soft" cations giving side-on binding. This is the general pattern that occurs in other cases, although it is particularly helpful to see it in a homologous series such as we have described here. The propensity of cyanides to bind end-on to hard metal cations and, in particular, transition metal cations (cf., structures of the Prussian Blue type) is very well known and needs no further elaboration.[12] Among simple alkali metal cyanide compounds, examples of "end-on" cyanide coordination are known for Li^+,[13] Na^+,[14] and K^+.[15] Examples of side-on cyanide coordination are also known with all of these cations and appear to become more common as the radius of the metal ion increases.[16] For Rb^+ and Cs^+, the cyanide-based coordination chemistry is dominated by the metal ions occupying the cavities between the layers in Prussian Blue lattices (or defect analogues), which involves weak side-on electrostatic interactions of the cyanide ligands with the alkali metal cation.[17]

In the next two parts of the paper, we look at the consequences of these interactions for the photophysical properties of $[Ru(bipy)(CN)_4]^{2-}$ both in the solid state and in solution.

(ii) Solid-State Luminescence Properties of the $[Ru(bipy)(CN)_4]^{2-}$ Salts. To see the solid-state luminescence of $[Ru(bipy)(CN)_4]^{2-}$ in the absence of interactions with additional metal cations, we first examined a powdered sample of the compound $(PPN)_2[Ru(bipy)(CN)_4]\cdot xH_2O$ (PPN^+ is the cation $\{Ph_3P{=}N{=}PPh_3\}^+$), which has been reported before by Evju and Mann.[18] We observed a weak luminescence maximum at 690 nm. Evju and Mann reported that the luminescence emission maximum for this compound varied from 815 nm (very weak) if the sample is strictly anhydrous, to 655 nm (much more intense) when exposed to air saturated with water vapor; this behavior parallels the solvatochromic behavior of $[Ru(bipy)(CN)_4]^{2-}$,[1−3] with the occurrence of hydrogen bonding to water molecules in the lattice of $(PPN)_2[Ru(bipy)(CN)_4]\cdot xH_2O$ correlating with higher energy and more intense luminescence.[18] Our observation of weak luminescence centered at 690 nm is entirely consistent with this and suggests an intermediate hydration state for our sample, which we did not shield from atmospheric moisture. The time-resolved luminescence decay from this sample fitted well to a double exponential decay with lifetime components of 82 ns (major component) and 361 ns (minor component). Given the inhomogeneity of the sample, with $[Ru(bipy)(CN)_4]^{2-}$ anions hydrated to different extents, the presence of two components with different lifetimes for the luminescence is not surprising. In addition, it is a known feature of solid-state samples that luminescence decay may not be single exponential because of microenvironmental heterogeneity, with different molecules having different orientations and local environments.[19] This phenomenon is likely to be particularly significant for compounds where solvation is strong, such as cyanometallates,[19] and we have frequently observed it.[11] For comparison, we note that the luminescence lifetime of $[Ru(bipy)(CN)_4]^{2-}$ in (isotropic) aqueous solution, that is,

(12) Dunbar, K. R.; Heintz, R. A. *Prog. Inorg. Chem.* **1997**, *45*, 283.
(13) (a) Bu, X. H.; Gier, T. E.; Stucky, G. D. *Acta Crystallogr., Sect. C* **1996**, *52*, 14. (b) Markley, T. J.; Toby, B. H.; Pearlstein, R. M.; Ramprasad, D. *Inorg. Chem.* **1997**, *36*, 3376.
(14) Parise, A. R.; Piro, O. E.; Castellano, E. E.; Olabe, J. A. *Inorg. Chim. Acta* **2001**, *319*, 199.
(15) Yuan, A.; Zou, J.; Li, B.; Zha, Z.; Duan, C.; Liu, Y.; Xu, Z.; Keizer, S. *Chem. Commun.* **2000**, 1297.
(16) (a) Buljan, A.; Alemany, P. *J. Phys. Chem.* **1997**, *101*, 1393. (b) Widmann, A.; Kahlert, H.; Petrovic-Prelevic, I.; Wulff, H.; Yakhmi, J. V.; Bagkar, N.; Scholz, F. *Inorg. Chem.* **2002**, *41*, 5706. (c) Contakes, S. M.; Rauchfuss, T. B. *Chem. Commun.* **2001**, 553. (d) Contakes, S. M.; Rauchfuss, T. B. *Angew. Chem., Int. Ed.* **2000**, *39*, 1984.
(17) (a) Rowe, J. M.; Rush, J. J.; Lüty, F. *Phys. Rev. B* **1984**, *29*, 2168. (b) Ohkoshi, S.; Tokoro, H.; Hashimoto, K. *Coord. Chem. Rev.* **2005**, *249*, 1830. (c) Kuhlman, M. L.; Rauchfuss, T. B. *J. Am. Chem. Soc.* **2003**, *125*, 10084. (d) Papanikolaou, D.; Margadonna, S.; Kosaka, W.; Ohkoshi, S.; Brunelli, M.; Prassides, K. *J. Am. Chem. Soc.* **2006**, *128*, 8358.
(18) Evju, J. K.; Mann, K. R. *Chem. Mater.* **1999**, *11*, 1425.
(19) Castelli, F.; Forster, L. F. *J. Am. Chem. Soc.* **1973**, *95*, 7223.

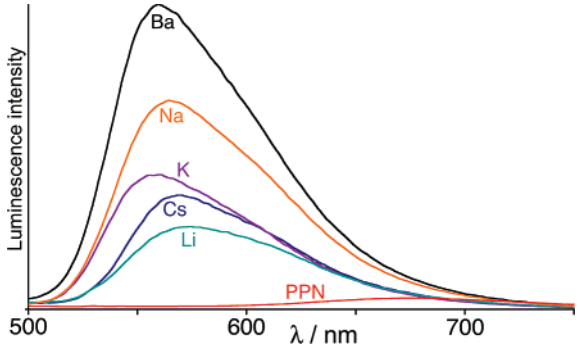

Figure 13. Solid-state luminescence spectra of various salts of $[Ru(bipy)(CN)_4]^{2-}$ recorded under identical conditions; the cations are indicated on the spectra.

hydrated but not interacting with any additional metal ions, is about 100 ns.[1−5]

All of the alkali metal and alkaline earth metal salts showed, as microcrystalline powders, the characteristic luminescence from the ^{3}MLCT state of the $[Ru(bipy)(CN)_4]^{2-}$ in the range 560−575 nm and with much greater intensity than that observed for $(PPN)_2[Ru(bipy)(CN)_4]\cdot xH_2O$ (Figure 13). Given that the luminescence maximum for fully hydrated solid $(PPN)_2[Ru(bipy)(CN)_4]\cdot xH_2O$ is at 655 nm,[18] the substantial blue-shift observed in the metal salts can be ascribed to the interactions of the cyanide ligands with the group 1A and 2A metal cations. This interaction results in an additional blue-shift in the ^{3}MLCT luminescence of 2100−2600 cm^{-1} as compared to the hydrated salt, depending on the metal cation; this "metallochromism" is accordingly similar in principle to but greater in magnitude than the solvatochromism for these compounds,[1−3] and greatly extends the range over which the ^{3}MLCT energy of the $[Ru(bipy)(CN)_4]^{2-}$ luminophore can be tuned.

From the spectra in Figure 13, we can see that there is no simple correlation between the energy of the emission maximum and the Lewis acidity of the metal countercation, with the Li^+ salt apparently being anomalous as it has the lowest energy emission maximum of this series (575 nm), despite the fact that the Li^+ cation has the highest charge density of those used. This may be explained with reference to the crystal structure. Li^+ is so Lewis-acidic that it interacts preferentially with water molecules in the crystal rather than the softer cyanide ligands. One of the Li^+ ions in the crystal exists as a $[Li(H_2O)_4]^+$ unit and does not directly interact with the $[Ru(bipy)(CN)_4]^{2-}$ at all, and each $[Ru(bipy)(CN)_4]^{2-}$ interacts with only two Li^+ ions. In contrast, although K^+ is a softer cation, each $[Ru(bipy)(CN)_4]^{2-}$ unit interacts directly with five K^+ ions (Figure 3), so the total effect is larger and the luminescence from the K^+ salt is at 561 nm. In the Ba^{2+} salt, like the Li^+ salt, each metal complex anion interacts with only two cations, but the higher charge of Ba^{2+} results in a more blue-shifted luminescence than for the Li^+ salt (560 nm). In the Cs^+ salt, like the K^+ salt, there are numerous cyanide/M^+ interactions, but the softer nature of the Cs^+ cation results in lower-energy luminescence (570 nm vs 561 nm). Thus, the luminescence spectra may be rationalized by taking into account both the Lewis acidity of the metal cation and the number of interactions between the metal cations and the $[Ru(bipy)(CN)_4]^{2-}$ anion as seen in the crystal structures.

The luminescence lifetimes of the solid-state materials show a similar trend (Table 1), with the higher-energy emitters having the longer lifetimes, up to 1.57 μs for the Ba^{2+} salt (λ_{em} = 560 nm) and down to 608 ns for the Li^+ salt (λ_{em} = 575 nm). For the reasons mentioned above, we do not always observe simple single-exponential decay kinetics for the luminescence from microcrystalline samples, and in some cases a fit to two components is clearly desirable. Overanalysis of these numbers is therefore not appropriate, but the general pattern is clear, and all of the lifetimes are much longer than for hydrated $[Ru(bipy)(CN)_4]^{2-}$ in aqueous solution[1−5] or in the solid state.[18]

Table 1. Luminescence Data for $[Ru(bipy)(CN)_4]^{2-}$ Salts in the Solid State and $(PPN)_2[Ru(^tBu_2bipy)(CN)_4]^{2-}$ in MeCN Solution in the Presence of Additional Metal Cations

	$[Ru(bipy)(CN)_4]^{2-}$ salts		$[Ru(^tBu_2bipy)(CN)_4]^{2-}$ adducts in solution		
cation	λ_{em} (solid)/ nm	τ (solid)/ ns	λ_{em} (MeCN)/ nm	τ (MeCN)/ ns	ϕ (MeCN)
Li^+	575	608	619	50, 120	*a*
Na^+	566	1410	630	215, 630	0.013
K^+	561	504, 1264	644	63, 127	0.003
Cs^+	570	686, 1188	646	72, 161	0.001
Ba^{2+}	560	1565	583	156, 1400	0.07
Zn^{2+}	*b*	*b*	537	285, 730	0.012
$(PPN)^+$	688	82, 361	∼800	12	*c*

[a] The intensity of luminescence in solution generated by addition of Li^+ ions was found to be somewhat variable according to the batch of the Li^+ salt used, possibly because of differing moisture contents (see refs 20 and 21). [b] The Zn(II) salt of $[Ru(bipy)(CN)_4]^{2-}$ could not be isolated as a pure crystalline material. [c] Very weak.

(iii) Solution Luminescence Properties of $[Ru(^tBu_2bipy)(CN)_4]^{2-}$ in the Presence of Different Metal Cations. We were interested to see if the same effect could be observed in solution, which would allow fine-tuning of the ^{3}MLCT energy of $[Ru(bipy)(CN)_4]^{2-}$ by addition or removal of metal ions of different Lewis acidity. We therefore performed a series of spectroscopic titrations, monitoring changes in luminescence emission wavelengths and lifetimes of $[Ru(^tBu_2bipy)(CN)_4]^{2-}$ in MeCN on addition of small aliquots of various soluble metal salts. We used $[Ru(^tBu_2bipy)(CN)_4]^{2-}$, containing the ligand 4,4′-di(*t*-butyl)-2,2′-bipyridine, because of its much higher solubility than $[Ru(bipy)(CN)_4]^{2-}$, which tended to precipitate out of MeCN on addition of excess amounts of metal cations such as Li^+ and Zn^{2+}. MeCN is a powerful enough solvent to dissolve many metal salts, but is not a hydrogen-bond donor (so will not interact significantly with the cyanide groups of the anion)[3] and is a poor ligand for the metal cations used in this study and so will not prevent them from binding to the cyanide groups.

We first examined the behavior of $(PPN)_2[Ru(^tBu_2bipy)(CN)_4]$ in the presence of Cs^+, using a 10^{-5} M solution of $(PPN)_2[Ru(^tBu_2bipy)(CN)_4]$ in MeCN, which shows the characteristic[1−3] two ^{1}MLCT absorptions at 529 and 368 nm. Addition of small portions of $Cs(BPh_4)$ (dissolved in MeCN) resulted in a slow blue-shift of these transitions, which was still continuing after addition of 100 equiv of $Cs(BPh_4)$, at which point they had reached 464 and 344 nm, respectively [Figure 14a]. This is much less than the changes that would occur in water, where the lowest ^{1}MLCT absorption is blue-shifted to ∼400 nm.[1−3] These shifts of the ^{1}MLCT absorption maxima to higher energy in the presence of Cs^+ were mirrored by changes in luminescence [Figure 14b]. In MeCN, $(PPN)_2[Ru(^tBu_2bipy)(CN)_4]$ shows very weak (barely detectable) luminescence at

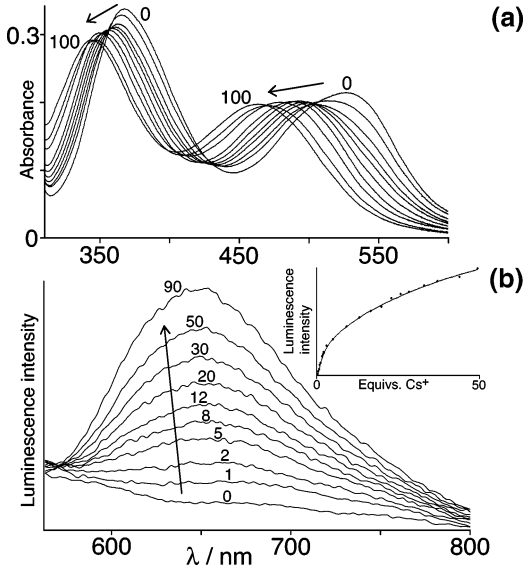

Figure 14. Changes in (a) UV/vis absorption spectra and (b) luminescence spectra of $(PPN)_2[Ru(^tBu_2bipy)(CN)_4]$ in MeCN during addition of successive portions of $Cs(BPh_4)$ (the number of equivalents added is shown on each curve). The inset to (b) shows the change in luminescence peak intensity as a function of added Cs^+ concentration, which was used to extract the two stepwise association constants (see main text); the dots are measured data points, and the line is the calculated best fit using the values for K_1 and K_2 given in the text.

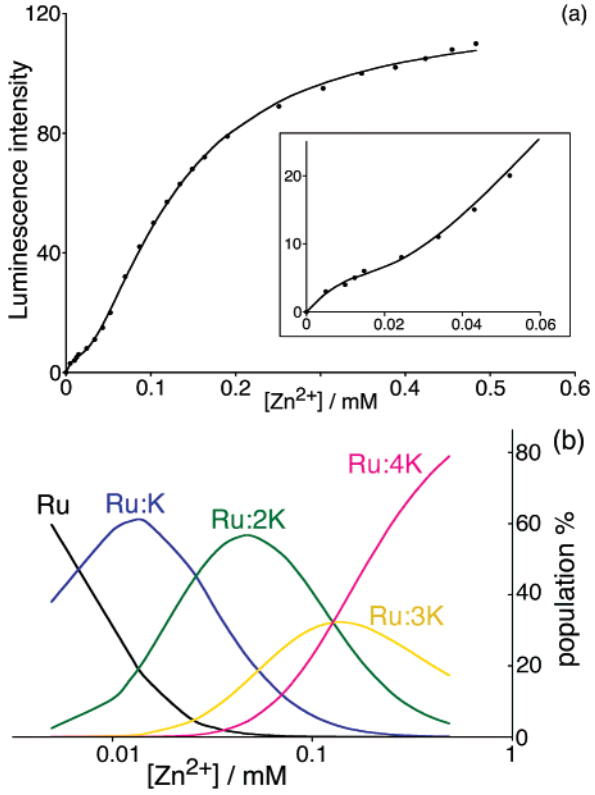

Figure 15. (a) The growth of luminescence during the titration of $(PPN)_2[Ru(^tBu_2bipy)(CN)_4]$ with KPF_6 in MeCN (10^{-5} M); the dots are experimental data, and the solid line is the best fit calculated on the basis of a 4:1 K^+:$[Ru(^tBu_2bipy)(CN)_4]^{2-}$ model, as discussed in the main text. The inset contains an expansion of the early part of the graph in part (a). (b) Calculated speciation diagram for the K^+:$[Ru(^tBu_2bipy)(CN)_4]^{2-}$ adducts during the titration (see Experimental Section for details).

~800 nm.[1−5,20,21] As $Cs(BPh_4)$ was added, a ^{3}MLCT luminescence band at 646 nm from $[Ru(^tBu_2bipy)(CN)_4]^{2-}$ appeared and steadily gained intensity during the titration; as with the blue-shift of the ^{1}MLCT absorptions in the UV/vis spectrum, this growth of luminescence was still continuing after the addition of 100 equiv of $Cs(BPh_4)$. The appearance of luminescence is clearly associated with cyanide/Cs^+ interactions in solution, which increase the ^{3}MLCT energy and luminescence intensity, exactly as observed in the solid state. A plot of luminescence intensity versus amount of added $Cs(BPh_4)$ shows a clear decrease in gradient after the addition of about 5 equiv [Figure 14b, inset] indicative of two binding events occurring of which the first is stronger than the second. These data fitted well to a 1:2 host:guest binding isotherm with microscopic association constants of $K_1 = 3.1 \times 10^4$ M^{-1} and $K_2 = 2.7 \times 10^3$ M^{-1} for binding of the first and second Cs^+ ions respectively.[22,23] The order of magnitude decrease from K_1 to K_2 implies that binding of the second Cs^+ ion is hindered by electrostatic repulsion from the first one.

There are two other points of significance that come out of this fitting. First, at the point we stopped the titration, after 100 equiv of $Cs(BPh_4)$, still only about half of the $[Ru(^tBu_2bipy)(CN)_4]^{2-}$ anions are interacting with Cs^+ ions. The projected end-point for the growth of luminescence after binding two Cs^+ ions is about double what is shown in Figure 14, and binding of further Cs^+ ions (albeit with, presumably, even weaker association constants) would cause a further gradual increase in luminescence until saturation occurs. However, at the concentration we used (10^{-5} M), only two binding events can be discerned. Second, the effects on luminescence intensity of binding the first and then the second Cs^+ ion are not equivalent. Of the total luminescence intensity that would arise from binding two Cs^+ ions, only about 20% arises from the first binding event, with the remaining 80% of the luminescence intensity arising when the second Cs^+ ion binds. In contrast, inspection of the UV/vis data shows that the effects of the two Cs^+ ions on the absorption spectrum of $[Ru(^tBu_2bipy)(CN)_4]^{2-}$ are approximately additive. Binding of the first Cs^+ ion causes a blue-shift of the lowest ^{1}MLCT band from 529 to ~490 nm (a 1500 cm^{-1} shift, estimated from curve fitting of the UV/vis spectral data as a function of added Cs^+), and binding of the second Cs^+ ion causes an additional blue-shift of 1800 cm^{-1} (from

(20) $[Ru(bipy)(CN)_4]^{2-}$ is sensitive to tiny traces of water in "anhydrous" solvents (ref 21) because of preferential solvation of the anion by the hydrogen-bonding water molecules; concentrations of water as low as 50 ppm were found to have a disproportionately large effect on the absorption spectrum. We found that solutions of $(PPN)_2[Ru(^tBu_2bipy)(CN)_4]$ in MeCN generally exhibited an extremely weak feature in the luminescence spectrum between 600 and 650 nm, comparable in magnitude to the expected weak band at ~800 nm, which we ascribe to selective solvation of the anion by traces of water, and it explains why the emission spectrum in Figure 16b before addition of any Cs^+ is not base-line flat in this region. This was completely dwarfed by the much stronger (orders of magnitude) increase in ^{3}MLCT luminescence on addition of metal salts and is for our purposes negligible.

(21) Pinheiro, C.; Lima, J. C.; Parola, A. J. *Sens. Actuators, B* **2006**, *114*, 978.

(22) These microscopic association constants K^{mic} are corrected for the statistical effect of there being two binding sites available for the first event but only one for the second, which would otherwise result in an additional factor of 4 difference between K_1 and K_2 for binding to two equivalent, non-interacting sites. With this factor removed, the order of magnitude difference between the microscopic K_1 and K_2 values quoted reflects a real decrease in the affinity of the cyanoruthenate anion for the second equivalent of Cs^+ as compared to the first, arising from electrostatic or steric factors.

(23) The fit is relatively insensitive to K_1 because, as will be seen from Figure 14b, the first few data points form a nearly linear sequence such that any value of K_1 that is comparable to, or larger than, the reciprocal of the concentration will give a reasonable fit to the early part of the curve. The value for K_2 is accordingly more reliable. The important points are that (i) two distinct binding events can clearly be discerned, and (ii) K_1 is clearly much greater than K_2.

~490 to ~450 nm, the projected end-point of the titration after complete binding of two Cs^+ ions based on the same curve-fitting).

Titration of $(PPN)_2[Ru(^tBu_2bipy)(CN)_4]$ with Li^+, Na^+, and K^+ (as their hexafluorophosphate salts) gave similar behavior in the UV/vis spectra, although the end-points of the titrations were more easily reached than with Cs^+ because of higher association constants between $[Ru(^tBu_2bipy)(CN)_4]^{2-}$ and these more Lewis-acidic metal cations. In all cases, the two ^{1}MLCT absorption maxima were steadily blue-shifted and ended up in similar positions irrespective of the nature of the metal cation, that is, at ~440 nm for the lower-energy peak and 330 nm for the higher one after addition of a large excess of the alkali metal salt. Note that the projected end-point for the $[Ru(^tBu_2bipy)(CN)_4]^{2-}/Cs^+$ titration gave a value of 450 nm for the lowest-energy ^{1}MLCT transition, comparable to values actually observed with Li^+, Na^+, and K^+, which reached their end-points more quickly. In all cases, the interaction between the alkali metal cation and the cyanides of $[Ru(^tBu_2bipy)(CN)_4]^{2-}$ resulted in the "switching on" of the ^{3}MLCT luminescence, but in this case the energy and intensity of the luminescence was cation-dependent, with Li^+ generating the highest-energy luminescence and Cs^+ having the weakest effect among the alkali metal cations. The luminescence wavelengths of $[Ru(^tBu_2bipy)(CN)_4]^{2-}$ at the end of the titrations with alkali metal salts in MeCN were 619, 630, 644, and 646 nm for Li^+, Na^+, K^+, and Cs^+, respectively, with Na^+ generating the most intense luminescence ($\phi = 0.013$) and Cs^+ the weakest ($\phi = 0.001$) (cf., the solid-state luminescence spectra in Figure 13).

In these cases, however, a simple 2:1 binding isotherm was not observed, with the complexity of the graphs of luminescence intensity versus amount of added M^+ for M = Li, Na, and K indicating complicated speciation behavior in solution. The data obtained for the luminescence of $[Ru(^tBu_2bipy)(CN)_4]^{2-}$ titration with KPF_6 in MeCN are in Figure 15. The curve has a "double sigmoidal" shape with an increase in luminescence intensity during the addition of the first equivalent of K^+, which then starts to level off before another increase in intensity as excess K^+ is added, before the increase again starts to level off. This data could be fitted accurately on the basis of four distinct binding events, with a tightly bound 1:1 K^+:$[Ru(^tBu_2bipy)(CN)_4]^{2-}$ complex forming in the first instance ($K_1 = 9.2 \times 10^5$ M^{-1}) followed by three additional K^+ ions binding less strongly, all with an identical microscopic stepwise association constant of K_2 of 3.1×10^4 M^{-1} for formation of the 2:1, 3:1, and 4:1 complexes. This is reasonable if one allows that each additional K^+ ion that binds to a cyanide group of $[Ru(^tBu_2bipy)(CN)_4]^{2-}$ is also associated with its hexafluorophosphate counterion, such that effectively neutral KPF_6 ion-pairs are involved in the second, third, and fourth associations; this will remove any tendency for successive binding constants to decrease due to electrostatic factors. Significantly, it was not possible to fit the experimental data on the basis of 2:1 or 3:1 K^+:$[Ru(^tBu_2bipy)(CN)_4]^{2-}$ adducts; a 4:1 stoichiometry is the lowest that fits the observed data, and of course there are four externally directed cyanide ligands available for interaction with K^+ ions in solution. An interesting feature that arises from the fitting, and which is obvious from the luminescence intensity data obtained during the titration (Figure 15), is that most of the growth of luminescence intensity is associated with the later stages of the titration in which 3:1 and 4:1 K^+:$[Ru(^tBu_2bipy)(CN)_4]^{2-}$ adducts dominate. For the 1:1, 2:1, 3:1, and 4:1 species, the calculated fraction of the observed emission that arises is 7%, 7%, 48%, and finally 100% (i.e., a modest amount of luminescence following the first binding event; no additional increase following the second binding event; and large increases when each of the third and fourth K^+ ions bind). It is plausible that the large increase in luminescence at the later stages of the titration is associated with complete removal of cyanide/solvent interactions as they are replaced by cyanide/M^{n+} interactions. The calculated speciation diagram showing the distributions of species in solution during the titration is in Figure 15b. Exactly similar behavior is shown on titration of $[Ru(^tBu_2bipy)(CN)_4]^{2-}$ using $LiPF_6$ (see ESI), with $K_1 = 7.8 \times 10^6$ M^{-1} and each of the three subsequent microscopic association constants being 4.5×10^4 M^{-1}. Note that the K_1 and K_2 values calculated for Li^+, K^+, and Cs^+ both follow the order $Li^+ > K^+ > Cs^+$, which is entirely reasonable.

Time-resolved measurements during the titrations show that the luminescence from the alkali metal adducts of $[Ru(^tBu_2bipy)(CN)_4]^{2-}$ is clearly not single exponential, but in all cases can be fitted to at least two components. Given the presence during the titration of a mixture of adducts with different numbers of alkali metal cations bound to the cyanides of $[Ru(^tBu_2bipy)(CN)_4]^{2-}$ [cf., the speciation diagram in Figure 15b], this is not surprising. In addition, the fact that binding of M^+ can occur at either the axial or the equatorial cyanide positions of $[Ru(^tBu_2bipy)(CN)_4]^{2-}$, leading to a mixture of two possible isomers for a 1:1 M^+:$[Ru(^tBu_2bipy)(CN)_4]^{2-}$ adduct and three possible isomers for a 2:1 adduct, complicates the system further. The limiting lifetimes at the end of the titrations (in the presence of 100-fold excess of the alkali metal salt) are collected in Table 1. Of the alkali metal cation adducts, Na^+ generated the longest-lived luminescence with lifetimes of 630 and 215 nm for the two components; for Li^+, K^+, and Cs^+, the lifetimes were all much lower (<200 ns for the longer-lived component and <100 ns for the shorter-lived component). It is noticeable from both the luminescence lifetimes and the intensity measurements that Na^+ cations have the strongest effect among the alkali metal cations on the luminescence of $[Ru(^tBu_2bipy)(CN)_4]^{2-}$. On electrostatic grounds, Li^+ might have been expected to have the strongest effect, but, as we saw in the crystal structures, the particularly high Lewis acidity of Li^+ results in it being preferentially hydrated such that it will not interact strongly with the cyanide ligands of $[Ru(^tBu_2bipy)(CN)_4]^{2-}$ if there are traces of moisture present.

Using metal dications resulted in similar but more dramatic changes in the absorption and luminescence behavior of $[Ru(^tBu_2bipy)(CN)_4]^{2-}$. The changes in the UV/vis absorption spectrum of $(PPN)_2[Ru(^tBu_2bipy)(CN)_4]$ in MeCN on addition of small portions of $BaClO_4$ were much more rapid than with the alkali metal salts, with the two ^{1}MLCT transitions at 529 and 368 nm collapsing and being replaced by higher-energy transitions, one at 409 nm and the other as an unresolved area of increasing absorbance between 300 and 320 nm, on the edge of the strong UV absorptions [Figure 16a]. This is exactly comparable to the spectroscopic changes that would occur on replacement of MeCN by water[3] and much greater than the shifts observed on addition of the alkali metal salts (see above). These spectral changes were substantial with concentration of added Ba^{2+} up to addition of 1 equiv, indicative of an association

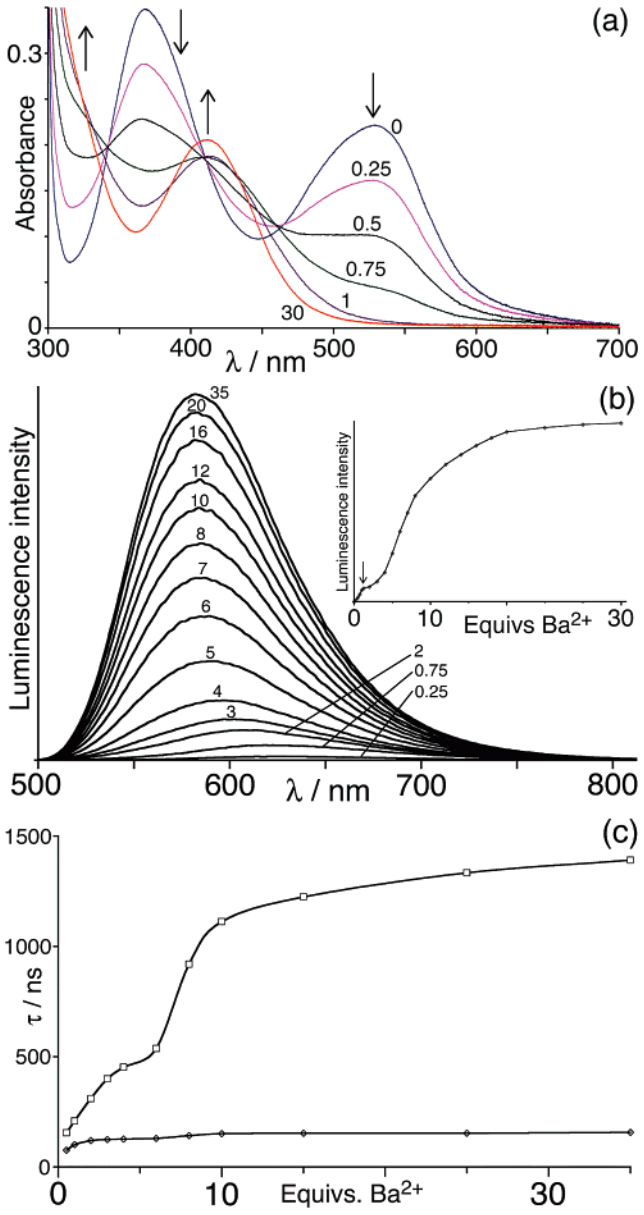

Figure 16. Spectroscopic changes occurring during titration of $(PPN)_2[Ru(^tBu_2bipy)(CN)_4]$ (10^{-5} M in MeCN) with $BaClO_4$. (a) Changes in UV/vis spectra (the number of equivalents of $BaClO_4$ added is shown on each spectrum); (b) the growth of ^{3}MLCT luminescence (again, the number of equivalents of $BaClO_4$ added is shown on each spectrum) with (inset) a plot of luminescence intensity versus amount of added Ba^{2+}; and (c) the variation in lifetime of the two luminescence components versus amount of added Ba^{2+}.

constant that is high at the concentration used; that is, we can say that $K_1 \gg 10^5$ M^{-1}. Further additions of Ba^{2+}, beyond 1 equiv, resulted in less dramatic additional changes to the absorption spectrum, requiring a much greater addition of Ba^{2+} to have a comparable effect [cf. the difference between adding 1 and 30 equiv of Ba^{2+} on the absorption spectrum, Figure 16a]. This suggests that association of a second (and possibly subsequent) Ba^{2+} ion is considerably more difficult than the first, which is reasonable on simple electrostatic grounds and fits the pattern that we saw with K^+ and Li^+.

The shifts of the ^{1}MLCT absorption maxima to higher energy were mirrored by the appearance of strong ^{3}MLCT luminescence from $[Ru(^tBu_2bipy)(CN)_4]^{2-}$ during the titration [Figure 16b]. In MeCN, $(PPN)_2[Ru(^tBu_2bipy)(CN)_4]$ is essentially non-luminescent;[20,21] addition of small portions of $Ba(ClO_4)_2$ resulted in the appearance of a ^{3}MLCT luminescence band, initially at 625 nm, which, as more $Ba(ClO_4)_2$ was added, grew in intensity and shifted to higher energy, reaching a limiting value of 583 nm after the addition of ca. 30 equiv of Ba^{2+}. The final quantum yield for this luminescence is 0.07, nearly 3 times higher than $[Ru(bipy)_3]^{2+}$ under the same conditions and much higher than what was obtained with any of the alkali metal cations. A plot of the emission intensity versus the amount of added $Ba(ClO_4)_2$ [Figure 16b, inset] shows a smooth, near-linear increase in luminescence intensity until ca. 1 equiv of Ba^{2+} is added, after which there is a clear discontinuity, indicated by an arrow on the figure (cf., the behavior of the absorption spectra). After this point, the curve is sigmoidal, characteristic of an additional two more (at least) binding events. Again, this data fitted well to a 4:1 Ba^{2+}:$[Ru(^tBu_2bipy)(CN)_4]^{2-}$ model with a high first binding constant K_1 (2.4×10^6 M^{-1}) and smaller but equivalent values for the three subsequent microsocopic binding constants K_2 (1.2×10^5 M^{-1}); and, again, most of the growth of luminescence intensity is associated with the later stages of the titration where the 4:1 Ba^{2+}:$[Ru(^tBu_2bipy)(CN)_4]^{2-}$ dominates (see the Supporting Information for full details of this fitting and the speciation diagram).

Time-resolved measurements during this titration with Ba^{2+} again do not show simple single-exponential kinetics for the luminescence decay of $[Ru(^tBu_2bipy)(CN)_4]^{2-}$. At every point after the titration started, the luminescence decay could be fitted reasonably well to two components, whose lifetime values both smoothly increased as the amount of Ba^{2+} added increased [Figure 16c]. After addition of 0.5 equiv of Ba^{2+}, the two lifetime components were 76 and 155 ns; by the end of the titration, after addition of 30 equiv of Ba^{2+}, the two components were 157 and 1400 ns. This latter value is close to what was observed in the solid state for the Ba^{2+} salt of $[Ru(bipy)(CN)_4]^{2-}$ (see above). It is apparent that interaction of $[Ru(^tBu_2bipy)(CN)_4]^{2-}$ with Ba^{2+} ions in MeCN solution results in a substantial increase in its luminescence energy, intensity, and lifetime, to a much greater extent than can be achieved using the alkali metal cations and also to a greater extent that can be achieved by using water as a solvent.

The most dramatic changes of all in the absorption and luminescence spectra of $[Ru(^tBu_2bipy)(CN)_4]^{2-}$ in solution were obtained on addition of $Zn(ClO_4)_2 \cdot 6H_2O$ ions (Figure 17). The ^{1}MLCT absorption maxima of $[Ru(^tBu_2bipy)(CN)_4]^{2-}$ shifted from 529 and 367 nm in the absence of Zn^{2+}, to 370 and ~310 nm, respectively, in the presence of an excess of Zn^{2+}. This constitutes a blue-shift of >8000 cm^{-1} in the lowest-energy ^{1}MLCT absorption maximum. The much stronger effect on the absorption spectra of $[Ru(^tBu_2bipy)(CN)_4]^{2-}$ resulting from adding Zn^{2+} as compared to Ba^{2+} is in contrast to the behavior of the alkali metal salts, which all generated comparable (and much smaller) spectral blue-shifts in the ^{1}MLCT absorptions irrespective of the size of the metal cation. Strong ^{3}MLCT luminescence appeared and simultaneously increased in intensity and blue-shifted as more Zn^{2+} was added; the luminescence maximum at the end of the titration was 537 nm, a shift of ca. 6000 cm^{-1} as compared to the luminescence from MeCN in the absence of any added metal salts; this effectively defines the limits of the useful range over which the ^{3}MLCT energy of the $[Ru(^tBu_2bipy)(CN)_4]^{2-}$ luminophore can be tuned. The final

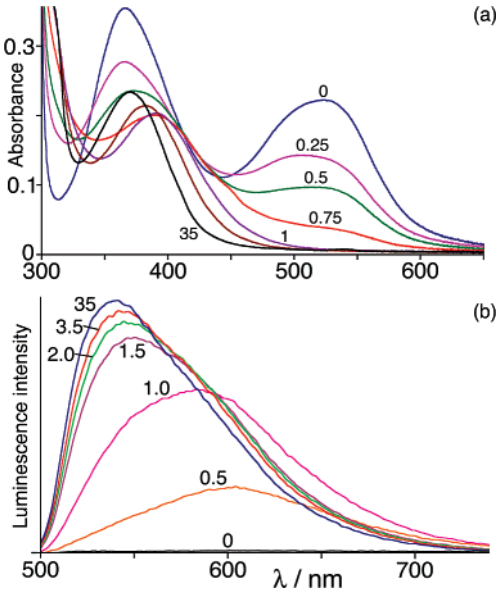

Figure 17. Spectroscopic changes occurring during titration of $(PPN)_2$-$[Ru(^tBu_2bipy)(CN)_4]$ (10^{-5} M in MeCN) with $Zn(BF_4)_2$. (a) Changes in UV/vis spectra (the number of equivalents of Zn^{2+} added is shown on each spectrum); (b) the growth of ^{3}MLCT luminescence (again, the number of equivalents of Zn^{2+} added is shown on each spectrum).

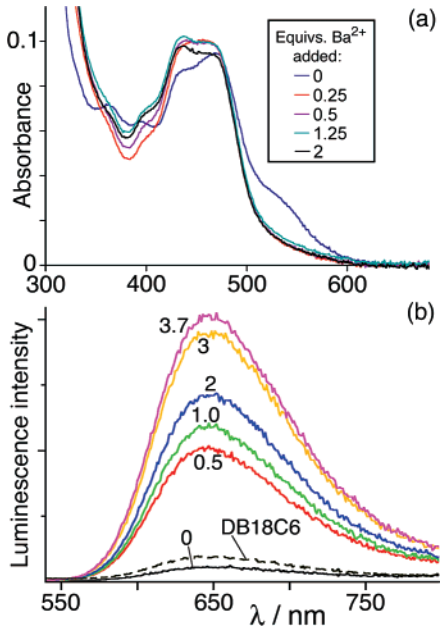

Figure 18. Changes in (a) absorption and (b) luminescence spectra of **1** in MeCN (8 μM) on titration with $BaClO_4$. In (b), the number of equivalents of added $BaClO_4$ is indicated on each spectrum; the black dashed line shows the spectrum after adding excess dibenzo-18-crown-6 after addition of $BaClO_4$ was complete.

quantum yield in aerated MeCN was 0.012, less than that obtained with Ba^{2+} even though the emission is at higher energy. The final emission lifetimes were 730 and 285 ns for the two components, that is, comparable to that obtained Na^+ and less than that with Ba^{2+}, in agreement with the quantum yields.

(iv) Use of the "Metallochromism" Effect To Switch the Direction of Photoinduced Energy Transfer in a [Ru(bipy)$_3$]$^{2+}$/[Ru(bipy)(CN)$_4$]$^{2-}$ Dyad. To exploit this effect for switching the direction of photoinduced energy transfer (PEnT) in a dyad, we prepared complex **1** by stepwise reaction of a known bis-bipyridyl bridging ligand (abbreviated L)[24] with $[Ru(bpyam)_2Cl_2]$ [bpyam = bipy-4,4′-$(CO_2NEt_2)_2$][25] to give mononuclear intermediate **2**, which was further reacted with $[Ru(CN)_6]^{4-}$ to give **1** (Chart 1). Complex **1** contains $\{Ru(bipy)(bpyam)_2\}^{2+}$ (hereafter, **Ru-bipy**) and $\{Ru(bipy)(CN)_4\}^{2-}$ (hereafter, **Ru−CN**) termini connected by a short covalent bridge. The neutral complex is highly soluble and was characterized satisfactorily by standard methods. Of particular note are the peak at *m*/*z* 692 in the ES mass spectrum, corresponding to $[\mathbf{1} + 2H]^{2+}$, and the IR spectrum that showed intense peaks corresponding to the CN vibrations of the **Ru−CN** terminus between 2000 and 2100 cm^{-1}, and the amide carbonyl vibration of the **Ru-bipy** terminus at ∼1640 cm^{-1}. Mononuclear complex **2**, a good model for the **Ru-bipy** terminus of **1**, shows the ^{3}MLCT luminescence characteristic of $[Ru(bipy)_3]^{2+}$ derivatives[26] at 640 nm in MeCN (τ = 340 ns, ϕ = 0.026), albeit at slightly lower energy due to the electron-withdrawing amide substituents. The diethylamide substituents are a convenient way of making the complex soluble in MeCN: a related $[Ru(bipy)_3]^{2+}$/$[Ru(bipy)(CN)_4]^{2-}$ dyad without such substituents that we described a few years ago was sparingly soluble in only DMSO and water.[5]

In MeCN solution, the absorption spectrum of **1** [Figure 18a] is essentially the sum of the spectra of the two chromophores,

Chart 1

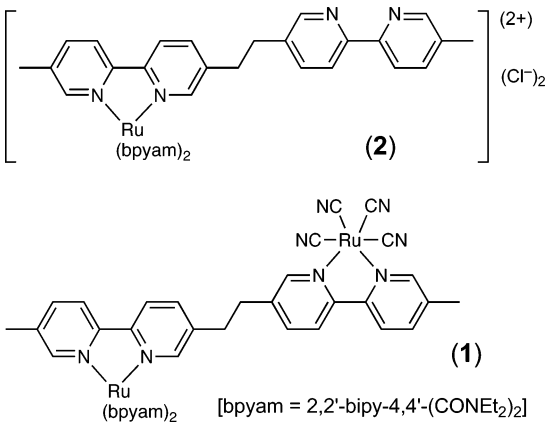

indicating very little ground-state interaction between the components, which is not surprising considering the saturated ethylene spacer connecting them. The main low-energy features are the ^{1}MLCT absorptions around 450 nm associated with the **Ru-bipy** terminus,[26] and the ^{1}MLCT absorption of the **Ru−CN** terminus, which is apparent as a shoulder at ∼530 nm. The luminescence is very weak, with a maximum just observable at 645 nm [Figure 18b, black line]. This can be ascribed to luminescence from the **Ru-bipy** unit of **1**, which is nearly completely quenched by energy transfer to the **Ru−CN** unit whose ^{3}MLCT state in MeCN is much lower in energy.[3,5] Any sensitized emission from the **Ru−CN** terminus, which is inherently very weak in MeCN and is expected at ∼800 nm,[1−5] is not detectable over this residual **Ru-bipy**-based emission.

To increase the excited-state energy of the **Ru−CN** terminus of **1**, we used $Ba(ClO_4)$, given the particularly strong effect of Ba^{2+} on the luminescence energy and lifetime of $[Ru(^tBu_2bipy)$-

(24) Lehn, J.-M.; Ziessel, R. *Helv. Chim. Acta* **1988**, 1511.
(25) Elliott, M. C.; Hershenhart, E. J. *J. Am. Chem. Soc.* **1982**, *104*, 7519.
(26) Juris, A.; Balzani, V.; Barigelletti, F.; Campagna, S.; Belser, P.; von Zelewsky, A. *Coord. Chem. Rev.* **1988**, *84*, 85.

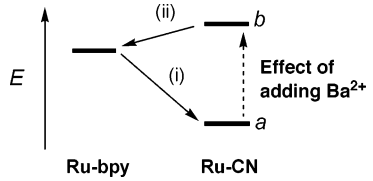

Figure 19. Qualitative energy-level diagram showing how the energy of the ^{3}MLCT state of the **Ru−CN** terminus of **1** changes from below that of the **Ru-bipy** terminus ((a), in MeCN) to above that of the **Ru-bipy** terminus ((b), on addition of Ba^{2+} ions). Consequently, the direction of PEnT reverses, as shown by the arrows labeled (i) (with no Ba^{2+}) and (ii) (with added Ba^{2+} ions). Process (i) results in quenching of **Ru-bipy**-based luminescence, whereas process (ii) results in its re-appearance, as shown in Figure 18b. For numerical values of energy levels, see main text.

$(CN)_4]^{2-}$ (described above). Addition of small portions of $Ba(ClO_4)_2$ to the solution of **1** results in the blue-shift of the 530 nm absorption shoulder, which is the ^{1}MLCT absorption associated with the **Ru−CN** terminus, following the arguments in section (iii) above. This band disappears under the stronger **Ru-bipy**-based absorptions as it blue-shifts. In the luminescence spectrum, there is a steady increase in the intensity of the 645 nm emission band, which reaches a maximum after about 4 equiv of Ba^{2+} has been added [Figure 18b]. The lifetime of this luminescence, measured at every point during the titration, is 360 (±10) ns,[27] and the quantum yield at the end of the titration is 0.022, both very similar to what was observed for the model complex **2** (and also to $[Ru(bipy)_3]^{2+}$).[26] This confirms that the luminescence arises from the **Ru-bipy** terminus of **1**, and not from the **Ru−CN** terminus affected by Ba^{2+} ions, from which the luminescence would be much higher in energy. Thus, the growth of this luminescence arises because the direction of PEnT in **1** is reversed as Ba^{2+} is added, according to the energy-level diagram shown in Figure 19. The presence of **Ru−CN → Ru-bipy** PEnT is also confirmed by the observation that the excitation spectrum of **1** is superimposable on its absorption spectrum; that is, those features in the absorption spectrum associated with the **Ru−CN** terminus lead, on excitation, to emission from the **Ru-bipy** terminus. The effect is almost completely reversible on addition of dibenzo-18-crown-6 to sequester the Ba^{2+} ions, with the emission from the **Ru-bipy** terminus now becoming quenched again [dashed line in Figure 18b] by energy transfer to the **Ru−CN** terminus whose ^{3}MLCT state is reduced in energy by removal of the Ba^{2+} ions.

For **Ru−CN → Ru-bipy** PEnT to be thermodynamically favorable, the ^{3}MLCT energy of the **Ru−CN** chromophore must be increased by interaction with Ba^{2+} ions to the extent that it now lies above the ^{3}MLCT energy of the **Ru-bipy** chromophore. $[Ru(^tBu_2bipy)(CN)_4]^{2-}$ can be considered a reasonable model for the **Ru−CN** terminus of **1**, because both bear two alkyl substituents attached to the $[Ru(bipy)(CN)_4]^{2-}$ core. In the presence of excess Ba^{2+}, the luminescence maximum of $[Ru(^tBu_2bipy)(CN)_4]^{2-}$ is at 583 nm [Figure 16b]; clearly, therefore, its ^{3}MLCT state lies above that of the **Ru-bipy** terminus of **1** whose luminescence maximum is at 645 nm. Making the approximation that the difference between the ^{3}MLCT energies of the two components is the same as the difference between their luminescence maxima, we have a gradient of 1600 cm^{-1} for **Ru−CN → Ru-bipy** PEnT in the presence of Ba^{2+}, which is sufficient for complete energy transfer to occur without significant thermal equilibration between the **Ru−CN**-based and **Ru-bipy**-based ^{3}MLCT states, which would occur if they were close together in energy.[5] In the absence of Ba^{2+}, in contrast, the ^{3}MLCT state of the **Ru−CN** terminus is much lower in energy; on the basis of the reported weak luminescence of $[Ru(bipy)(CN)_4]^{2-}$ at 780 nm in MeCN,[3] this would provide a gradient of 2600 cm^{-1} for **Ru-bipy → Ru−CN** PEnT, such that the strong **Ru-bpy**-based luminescence at 645 nm becomes quenched again when the Ba^{2+} ions are sequestered by dibenzo-18-crown-6. Thus, in dyad **1**, the direction of photoinduced energy transfer from one terminus to the other can be alternated back and forth by addition of, and then removal of, Ba^{2+} ions.

(27) The **Ru-bipy**-based luminescence that appears on addition of Ba^{2+} to **1** in MeCN solution has two components: the major component (~90%) has a lifetime of 360 (±10) ns, but there is also a minor component (~10%) with a lifetime of 100 (±10) ns. This may arise from the presence of major and minor alternate conformers of this flexible molecule.

Conclusions

The interaction of the cyanide ligands of $[Ru(bipy)(CN)_4]^{2-}$ with metal cations has been studied both in the solid state and in solution; these interactions are of great scope for the preparation of unusual coordination networks and for the modulation of the photophysical properties of $[Ru(bipy)(CN)_4]^{2-}$ over a wide range. The crystal structures of a range of salts of $[Ru(bipy)(CN)_4]^{2-}$ show that both "end-on" and "side-on" coordination of cyanides to additional metal cations such as Li^+, Na^+, K^+, Cs^+, and Ba^{2+} can occur, with the mode of coordination depending on the size and charge of the metal ion; "harder" metal cations favor end-on cyanide bridges, and "softer" cations favor side-on interactions with cyanides, at least in the solid state. These interactions raise the energy of the ^{3}MLCT state of the $[Ru(bipy)(CN)_4]^{2-}$ as compared to the situation in crystals with an organic cation $(PPN)^+$, resulting in intense, long-lived luminescence in the solid state. The interactions also occur in solution in a noncompetitive solvent (MeCN); addition of a range of metal salts to a solution of $(PPN)_2[Ru(^tBu_2bipy)(CN)_4]$ results in a blue-shift of the ^{1}MLCT absorptions, and the appearance of strong ^{3}MLCT luminescence whose energy and intensity depends on the nature of the metal cation (λ_{em} varies from 646 nm in the presence of Cs^+ to 537 nm in the presence of Zn^{2+}, with the highest quantum yield being 0.07 in the presence of Ba^{2+}). This ability to raise the ^{3}MLCT energy of the $[Ru(bipy)(CN)_4]^{2-}$ unit was exploited to switch the direction of energy transfer in a $[Ru(bipy)_3]^{2+}/[Ru(bipy)(CN)_4]^{2-}$ dyad in which the ^{3}MLCT energy of the $[Ru(bipy)(CN)_4]^{2-}$ terminus lies either below that of $[Ru(bipy)_3]^{2+}$ (in the absence of additional metal ions) or above it (in the presence of added Ba^{2+} ions).

The substantial changes in luminescence of $[Ru(^tBu_2bipy)(CN)_4]^{2-}$ in the presence of additional metal cations in solution, that is, the switching "on" of luminescence in the presence of a strongly binding cation such as Ba^{2+}, suggest possible applications of simple $[Ru(bipy)(CN)_4]^{2-}$ derivatives as luminescent sensors. In addition, the ability to vary the ^{3}MLCT energy of the chromophore over a range of about 6000 cm^{-1} means that there is great scope for using this "metallochromic" effect as a switching mechanism for controlling the flow of excited-state energy in polynuclear assemblies, as we have demonstrated in a simple dyad.

Experimental Section

General Details. The following compounds were prepared according to published procedures: bridging ligand L,[24] 2,2′-bipyridine-4,4′-$(CONEt_2)_2$ (bpyam),[25] $K_2[Ru(bipy)(CN)_4]$,[1b] $(PPN)_2[Ru(^tBu_2bipy)(CN)_4]$.[28] Ruthenium salts $RuCl_3 \cdot 3H_2O$ and $K_4[Ru(CN)_6]$ were kindly provided on loan by Johnson Matthey plc.

^1H NMR spectra were recorded on Bruker AC-250 or AMX2-400 spectrometers. Electrospray mass spectra were recorded on a Waters-LCT time-of-flight spectrometer; UV/vis spectra were measured on a Cary-50 instrument; IR spectra were measured as Nujol mulls or as compressed KBr pellets on a Perkin-Elmer Spectrum One instrument. Steady-state luminescence spectra were measured on a Perkin-Elmer LS50B fluorimeter, using a front surface accessory in the case of powder samples. For solution samples, excitation was performed at a wavelength where the absorbance of the sample was about 0.1. Luminescence lifetimes of the samples described in sections (ii) and (iii) of the Results and Discussion (i.e., salts of $[Ru(bipy)(CN)_4]^{2-}$ as microcrystalline powders, and measurements during solution titrations of $[Ru(^tBu_2bipy)(CN)_4]^{2-}$) were measured using an Edinburgh Instruments Mini-τ instrument fitted with a 405 nm pulsed diode laser as excitation source and a cooled Hamamatsu-R928 PMT detector; wavelength selection at the detector was by means of 50 nm bandpass filters. The luminescence properties of complexes **1** and **2** [section (iv) of the Results and Discussion] were recorded on an Edinburgh Instruments FLSP-920 spectrometer using a Xe lamp as the excitation source.

Syntheses of Different Salts of $[Ru(bipy)(CN)_4]^{2-}$. Crystalline samples of the salts with group 1A or 2A metal cations were grown by slow evaporation of an aqueous solution containing $K_2[Ru(bipy)(CN)_4] \cdot 3H_2O$ (20 mg, 41 μmol) and a large excess (10 equiv) of a group 1A or 2A metal salt in 3 cm^3 water. After several days, orange crystals appeared that were collected by filtration. Specific details for each one are as follows:

$Li_2[Ru(bipy)(CN)_4]$ was prepared as above using LiCl. FT-IR (cm^{-1}): 3472 (br), 2093 (sh), 2055 (sh), 1652 (br), 1465 (sh). Anal. Calcd for $Li_2C_{14}H_8N_6 \cdot (H_2O)_6$: C, 44.0; H, 5.2; N, 22.0%. Found: C, 43.7; H, 5.4; N, 21.8%. When a smaller excess of LiCl was used, some crystals of a different habit appeared that proved on crystallographic analysis to be the mixed salt **LiK[Ru(bipy)(CN)$_4$]** (see main text).

$Cs_2[Ru(bipy)(CN)_4]$ was prepared as above using CsCl. FT-IR (cm^{-1}): 3324 (br), 2055 (sh), 2027 (sh), 1462 (br), 1374 (sh). Anal. Calcd for $Cs_2C_{14}H_8N_6 \cdot (H_2O)_2$: C, 29.9; H, 2.1; N, 15.0%. Found: C, 29.5; H, 2.3; N, 14.6%.

$Na_2[Ru(bipy)(CN)_4]$ was prepared as above using NaCl. FT-IR (cm^{-1}): 3340 (br), 2055 (sh), 2022 (sh), 1637 (br), 1462 (sh), 1374 (sh). Anal. Calcd for $Na_2C_{14}H_8N_6 \cdot (H_2O)_6$: C, 40.6; H, 4.8; N, 2.3%. Found: C, 40.3; H, 5.0; N, 2.2%.

$Ba[Ru(bipy)(CN)_4]$ was prepared as above using $Ba(ClO_4)_2$. FT-IR (cm^{-1}): 3379 (br), 2088 (sh), 2049 (sh), 1652 (br), 1465 (sh). Anal. Calcd for $BaC_{14}H_8N_6 \cdot (H_2O)_6$: C, 33.2; H, 4.0; N, 16.6%. Found: C, 33.1; H, 4.2; N, 16.3%.

Synthesis of $Ru(bpyam)_2Cl_2$. A mixture of $RuCl_3 \cdot 3H_2O$ (2.62 g, 10.0 mmol), LiCl (3.25 g, 77 mmol, large excess), and bpyam (6.83 g, 19.2 mmol) in dry DMF (200 cm^3) was refluxed with stirring for 20 h, forming a brown solution. The solvent was distilled off, the residue was dissolved in CH_2Cl_2, and any residual solid was filtered off. This organic solution was washed with copious water (5 × 1 L) to remove the charged complex $[Ru(bpyam)_3]Cl_2$, which turns the aqueous phase orange. The remaining CH_2Cl_2 solution was evaporated in vacuo, and the purple product was purified by column chromatography on silica with CH_2Cl_2:MeOH (10:1). This yielded a purple solid product (6.11 g, 72%). ESMS *m*/*z* 845 $\{M - Cl\}^+$. ^1H NMR (250 MHz, $CDCl_3$): δ 1.1−1.3 (24H, m, CH_3), 3.3−3.6 (16H, m, CH_2), 6.92 (2H, dd, H6′), 7.56 (2H, dd, H5′), 7.64 (2H, d, H5), 8.03 (2H, d, H3′), 8.19 (2H, d, H3), 10.36 (2H, d, H6).

Synthesis of $[Ru(bpyam)_2(L)]Cl_2$ (2). A mixture of $Ru(bpyam)_2Cl_2$ (1.9164 g, 2.178 mmol) and silver nitrate (712 mg, 14.36 mol) in EtOH (60 cm^3) was heated to reflux for 30 min. The white AgCl precipitate was filtered off, and the bis-bipyridyl ligand L (837 mg, 2.287 mmol) was added to the filtrate. The reaction mixture was refluxed with stirring overnight, and then the solvent was removed in vacuo. Purification of the crude reaction product was achieved by column chromatography on Sephadex SP C-25 with a steadily increasing concentration of aqueous NaCl solution (0−0.4 M) as eluent. After evaporation of the water, excess NaCl was removed by dissolving the product in CH_2Cl_2 and filtering through celite. This yielded a dark red product (1.86 g, 68%). The product is hygroscopic. ESMS *m*/*z* 588.4 $\{M - 2Cl\}^{2+}$. Anal. Calcd for $RuC_{64}H_{74}N_{12}O_4Cl_2 \cdot 6H_2O$: C, 56.7; H, 6.4; N, 12.4%. Found: C, 56.3; H, 6.7; N, 12.3. ^1H NMR (250 MHz, CD_3OD): δ 1.08−1.35 (24H, m, amide C**H**$_3$CH$_2$), 2.25 (3H, s, bridging ligand CH_3), 2.45 (3H, s, bridging ligand CH_3), 2.75−3.15 (8H, m, amide CH_3C**H**$_2$), 3.35 (4H, s, bridging ligand CH_2CH_2), 3.53−3.67 (8H, m, CH_3C**H**$_2$), 7.10 (1H, s), 7.31 (1H, d), 7.50 (2H, m), 7.50 (1H, m), 7.57 (2H, dt), 7.65 (1H, d), 7.67 (1H, d), 7.79 (1H, d), 7.87 (1H, d), 7.94 (1H, d), 7.98 (1H, dd), 8.11 (1H, d), 8.12 (2H, d), 8.22 (1H, d), 8.49 (1H, t), 8.57 (1H, d), 8.63 (1H, d), 8.72 (2H, t), 8.79 (1H, d), 8.81(1H, d).

Synthesis of $[(CN)_4Ru(\mu\text{-}L)Ru(bpyam)_2]$ (1). A mixture of complex **2** (500 mg, 0.4 mmol) and $K_4[Ru(CN)_6] \cdot 3H_2O$ (197 mg, 0.421 mmol) was combined in H_2O:MeOH (1:1, 50 cm^3, pH 3.5 with H_2SO_4) and refluxed with stirring overnight to form a red-brown solution. After being cooled, the solution was neutralized with K_2CO_3, and the solvent was evaporated in vacuo. The residue was redissolved in CH_2Cl_2 and filtered through celite, yielding after evaportation of solvent a dark red-black powder (400 mg). The product was separated from unreacted starting material and polynuclear byproducts by preparative TLC on an alumina plate eluting with MeCN:H_2O:sat. aqueous KNO_3 (10:2:1), and was further purified by loading onto a short alumina column, eluting with CH_2Cl_2:MeOH (5:1), discarding the eluent and washing the alumina with water to recover the product. Evaporation of water afforded pure red-black product (150 mg, 30%). ESMS *m*/*z* 692 $\{M + 2H\}^{2+}$, 703 $\{M + Na + H\}^{2+}$. ^1H NMR (250 MHz, CD_3OD): δ 1.08−1.37 (24H, m, amide C**H**$_3$CH$_2$), 2.23 (3H, s, bridging ligand CH_3), 2.43 (3H, s, bridging ligand CH_3), 2.9−3.15 (6H, m, amide CH_3**CH**$_2$), 3.35 (4H, s, bridging ligand CH_2CH_2), 3.5−3.75 (10H, amide CH_3C**H**$_2$), 7.10 (1H, dd), 7.36 (1H, s), 7.41 (1H, s), 7.44 (2H, dt), 7.65−7.74 (2H, m), 7.80 (1H, d), 7.90 (1H, s), 7.93 (1H, s), 7.96−8.13 (5H, m), 8.52 (1H, d), 8.58−8.66 (3H, m), 8.75 (2H, s), 8.82 (1H, d), 9.12 (1H, d), 9.34 (1H, d). Elemental analyses were somewhat variable and consistent with the presence of a few water molecules of crystallization, which could not be completely removed by vacuum drying.

Stability Constant Calculations. The luminescence titration data were analyzed using purpose written software (by CAH) on an Apple Macintosh computer. The data obtained during titration with Cs^+ were fitted to a simple 2:1 host (Ru complex):guest (Cs^+ ion) model using a program that has been described previously.[29] The other three systems studied (Li^+, K^+, Ba^{2+}) show two distinct phases in the titration: formation of a tightly bound 1:1 complex, followed by weaker binding of additional metal ions. The speciation model used to fit the titration data therefore featured the formation of a 1:1 complex with an association constant K_1, followed by the formation of a 4:1 complex, with an identical microscopic stepwise association constant of K_2 for formation of the 2:1, 3:1, and 4:1 complexes, according to the scheme below.

(28) Derossi, S.; Adams, H.; Ward, M. D. *Dalton Trans.* **2007**, 33.

(29) Bisson, A. P.; Hunter, C. A.; Morales, J. C.; Young, K. *Chem.-Eur. J.* **1998**, *4*, 845.

$$M + L \leftrightarrow ML \qquad K_1 = K_{11}$$

$$ML + 3M \leftrightarrow M_4L \qquad K_2 = 0.33K_{11\rightarrow 21} = K_{21\rightarrow 31} = 3K_{31\rightarrow 41}$$

{where M represents the added metal cation (Li^+, Ba^{2+}, etc.) and L represents the "ligand" $[Ru(^tBu_2bipy)(CN)_4]^{2-}$}. Using simpler 2:1 and 3:1 models, it was not possible to fit the experimental titration curves, and a 4:1 stoichiometry is the lowest that is consistent with the measurements.

In this scheme, the concentrations of the complexes at any point in the titration are given by:

$$[ML] = K_1[M][L]$$

$$[M_2L] = 3K_1K_2[M]^2[L]$$

$$[M_3L] = 3K_1K_2^2[M]^3[L]$$

$$[M_4L] = K_1K_2^3[M]^4[L]$$

$$[ML_2] = K_1K_3[M][L]^2$$

The total concentrations of M and L are given by:

$$[L]_T = [M] + [ML] + [M_2L] + [M_3L] + [M_4L] + 2[ML_2]$$

$$[M]_T = [L] + [ML] + 2[M_2L] + 3[M_3L] + 4[M_4L] + [ML_2]$$

For a given set of association constants, K_1, K_2, and K_3, these simultaneous equations can be solved for the concentrations of all species using the iterative COGS algorithm,[30] and the calculated luminescence, I, for this system is then given by:

$$I = [L]I_L + [ML]I_{ML} + [M_2L]I_{M_2L} + [M_3L]I_{M_3L} + [M_4L]I_{M_4L} + 2[ML_2]I_{ML_2}$$

where I_L, I_{ML}, I_{M_2L}, I_{M_3L}, I_{M_4L}, and I_{ML_2} are the luminescence intensities for 100% formation of the relevant species.

The values of the association constants and the fully bound luminescence intensities of all of the species present were obtained by fitting the experimental titration data to the calculated luminescence intensity using a Simplex optimization procedure to minimize the sum of the squares of the differences between the calculated and experimental values.[31] This procedure optimizes the values of K_1, K_2, K_3, I_L, I_{ML}, I_{M_2L}, I_{M_3L}, I_{M_4L}, and I_{ML_2} from a given starting point, and the results are presented in the main text. The first phase of the binding isotherm is in the tight binding limit, and so it not possible to accurately determine the values of K_1 and K_3, but the best fits were obtained with K_1 values in the range 10^6-10^7 M^{-1} for all three systems, and a K_3 of 10^5-10^6 M^{-1} for the Ba^{2+} ML_2 complex.

X-ray Crystallography. Suitable crystals were grown by slow evaporation from aqueous solution as described above and were mounted in a stream of cold N_2 on a Bruker APEX-2 CCD diffractometer equipped with graphite-monochromatized Mo Kα radiation from a sealed-tube source. Details of the crystallographic, data collection, and refinement parameters, and selected structural parameters for all structures, are collected in the Supporting Information. After integration of the raw data and merging of equivalent reflections, an empirical absorption correction was applied on the basis of comparison of multiple symmetry-equivalent measurements.[32] The structures were solved by direct methods and refined by full-matrix least-squares on weighted F^2 values for all reflections using the SHELX suite of programs.[33] None of the refinements presented any significant problems, apart from $Na_2[Ru(bipy)(CN)_4]\cdot(H_2O)_9$ in which the Na atoms and several of the associated water ligands are disordered over two sites with 50% occupancy in each (see main text). In this series of structures, H atoms were added to coordinated and lattice water molecules only when both of them showed up clearly in a Fourier difference map using only low-angle data; they were then fixed in position with O−H distances of 0.85 Å.

Acknowledgment. We thank the EPSRC (UK) for financial support.

Supporting Information Available: Full crystallographic details, including data collection/refinement details and tables of bond distances and angles for the crystal structures; crystallographic CIF files; and details of the luminescence titrations of $[Ru(^tBu_2bipy)(CN)_4]^{2-}$ with Li^+ and Ba^{2+} and the calculated association constants and speciation diagrams. This material is available free of charge via the Internet at http://pubs.acs.org.

JA068436N

(30) Quinn, G. W.; Taylor, D. M. *Analyst* **1992**, *117*, 689.

(31) Nelder, J. A.; Mead, R. *Comput. J.* **1965**, *7*, 308.

(32) Sheldrick, G. M. *SADABS: A program for absorption correction with the Siemens SMART system*; University of Gottingen, Germany, 1996.

(33) *SHELXTL program system version 5.1*; Bruker Analytical X-ray Instruments Inc., Madison, WI, 1998.